POLY(L-LYSINE)-GRAFTED-POLY(ETHYLENE GLYCOL) NANOPARTICLES

FOR DELIVERY OF PROTEINS:

EFFECTS OF STIMULUS-RESPONSIVE CROSSLINKING

AND TUNABLE MILLIFLUIDIC ASSEMBLY

By

JOSHUA SEABERG

Bachelor of Science in Chemical Engineering

Oklahoma State University

Stillwater, Oklahoma

2018

Submitted to the Faculty of the
Graduate College of the
Oklahoma State University
in partial fulfillment of
the requirements for
the Degree of
MASTER OF SCIENCE
May, 2020

POLY(L-LYSINE)-GRAFTED-POLY(ETHYLENE GLYCOL) NANOPARTICLES

FOR DELIVERY OF PROTEINS:

EFFECTS OF STIMULUS-RESPONSIVE CROSSLINKING

AND TUNABLE MILLIFLUIDIC ASSEMBLY

Thesis Approved:

Joshua Ramsey

Thesis Adviser

Heather Fahlenkamp

Clint Aichele

ACKNOWLEDGEMENTS

I would like to acknowledge the virus known as COVID-19 for giving me the time to complete this thesis.

Name: JOSHUA SEABERG

Date of Degree: MAY 2020

Title of Study: POLY(L-LYSINE)-GRAFTED-POLY(ETHYLENE GLYCOL)

NANOPARTICLES FOR DELIVERY OF PROTEINS: EFFECTS OF STIMULUS-

RESPONSIVE CROSSLINKING AND TUNABLE MILLIFLUIDIC ASSEMBLY

Major Field: CHEMICAL ENGINEERING

Abstract: Polymeric nanoparticles have drawn attention for their ability to enhance the efficacy of therapeutic proteins through reduced immunogenicity and extended circulation time. Nevertheless, nanoparticle drug delivery systems face hurdles in both application and production. The challenge of selective delivery to clinically-relevant locations can be addressed by integrating stimulus-responsive moieties into the nanoparticle structure. This study examined the effects of crosslinking nanoparticles of bovine serum albumin (BSA) encapsulated within poly(L-lysine)-grafted-poly(ethylene glycol) (PLL-g-PEG) with redox-responsive 3,3'-dithiobis(sulfosuccinimidyl propionate) (DTSSP) to achieve selective destabilization in a tumor environment. A library of DTSSP-crosslinked nanoparticles (DTSSP NPs) was formed with varying copolymer to protein (C:P) and crosslinker to protein (X:P) ratios, and each formulation was characterized by size, polydispersity index, and encapsulation efficiency. DTSSP NPs showed stability in the presence of serum and proteases, but rapidly destabilized when exposed to dithiothreitol. For therapeutic nanoparticle production, continuous processes have been proposed to overcome the challenges of poor scalability and few control parameters associated with batch synthesis. A millifluidic process was developed to encapsulate (BSA) in PLL-g-PEG through electrostatic self-assembly. The millifluidic process produced tunable nanoparticles (13 - 300 nm) that fully encapsulated the protein, retained its activity, and protected it from proteases. This thesis presents the utility of stimulus-responsive crosslinking for selective nanoparticle stabilization and proposes a millifluidic synthesis process for the production of nanoparticle drug delivery systems that may be foundational to the clinical translation of polymer-protein nanoparticles.

TABLE OF CONTENTS

LIST OF TABLES

LIST OF FIGURES

CHAPTER I

INTRODUCTION

Proteins are ubiquitous biomolecules that perform specific biological functions; as such, certain proteins have been effective in treating diseases ranging from pulmonary embolism to cancer and arthritis [1, 2]. Despite this efficacy, systemic administration of proteins in therapeutic applications faces multiple challenges, including side effects, protein denaturation, weak intracellular delivery, and rapid *in vivo* clearance [3, 4]. Consequently, much effort has been expended developing drug delivery systems capable of shielding therapeutic proteins from clearance by the immune system while enhancing site-specific action.

Therapeutic proteins are broadly defined as proteins that have been developed for pharmaceutical use, and they display benefits including high substrate specificity and utilization of existing biological processes [5]. Nevertheless, much protein functionality is intrinsically tied to its conformation, and thus the aggregation and denaturation that may occur when administered medicinally can detrimentally affect therapeutic efficacy [6, 7]. Furthermore, immunogenicity is frequently a problem, and most proteins are limited in their ability to transverse the cellular membrane which constrains their effective domain to the extracellular space [4, 5]. As nanotechnology holds promise to overcome these challenges, investigations into delivery of therapeutic proteins using nm-scale carriers have blossomed. A common approach toward

overcoming these challenges is to use biocompatible polymers to shield proteins from identification and elimination by the immune system [8]. These polymer-protein nanoparticles show potential for drug delivery applications due to their versatility from trans-membrane delivery to active cell targeting [9-12]. In many cases, a hydrophilic polymer such as poly(ethylene glycol) is utilized to reduce non-specific interactions between the nanoparticle and the biological environment, which reduces the immune response and increases the time a therapeutic may spend *in vivo* before clearance [13-15]. Accordingly, polymer-protein nanoparticles show potential to address the shortcomings of therapeutic protein administration.

An advantage of utilizing polymers in drug delivery applications is that stimulus-responsive moieties can be included within the polymer structure. These moieties respond to local environmental conditions to trigger a conformational change or induce particle destabilization leading to protein release [16]. This latter development is of considerable interest as it allows for effective therapeutic application through reduced immune clearance while maximizing the efficacy of the encapsulated protein in the desired location [17]. Polymer-protein delivery systems have been sensitized to both endogenous and exogenous triggers ranging from pH to ultrasound [18-22].

While there are numerous designs for medically-relevant polymer-protein nanoparticles, the majority are made in small scale batch processes. Bulk mixing is a straightforward strategy for particle development, but it does not allow for fine control over product characteristics [23]. Batch processes offer few factors for tuning the synthesis conditions, which can lead to difficulty controlling the size and size distribution of the nanoparticles [23]. Additionally, batch processes present challenges with scalability, which can limit the clinical relevance of effective but difficult-to-manufacture delivery systems [24, 25]. As such, development of a continuous process for the synthesis of polymer-protein nanoparticles shows potential to improve both the tunability and scalability of current nanoparticle formation processes.

Previously, cationic poly(L-lysine) was grafted with poly(ethylene glycol) (PLL-g-PEG) and utilized to encapsulate bovine serum albumin through electrostatic self-assembly in a small scale batch process [26]. The initial aim of this research was to confer redox-responsive properties on the PLL-g-PEG nanoparticles through crosslinking with 3,3'-dithiobis(sulfosuccinimidyl propionate) (DTSSP). DTSSP contains a disulfide to enable nanoparticle destabilization and protein release in a reductive environment. Bovine serum albumin (BSA), selected for its stability, was utilized as a model protein to determine the effect of DTSSP crosslinking on the size and encapsulation efficiency of a library of self-assembled nanoparticles. One nanoparticle formulation displaying favorable properties was subsequently characterized for retention of protein activity, stability in the presence of serum and proteases, and destabilization in a reductive environment.

The second aim of this research was to develop a continuous process for producing nanoparticles of BSA encapsulated within PLL-g-PEG. A system was developed using a syringe pump to feed solutions containing BSA and PLL-g-PEG through a millifluidic channel. Electrostatic self-assembly was stimulated using ultrasound to induce controlled mixing in a laminar flow regime. The objective of this research was to present a method capable of producing stable, tunable, polymer-protein nanoparticles using a continuous millifluidic process. The diameters of the nanoparticles were tunable by varying the feed flow rate, tubing material, and ultrasonication power. Millifluidic nanoparticles were characterized by morphology, polydispersity index, ζ-potential, retention of enzymatic activity, particle stability, and encapsulation efficiency.

CHAPTER II

REVIEW OF LITERATURE

Drug-related research has long upheld the goal of developing novel therapeutics, with primary

aims including the enhancement and discovery of new and existing active pharmacological agents

[27, 28]. In recent decades, however, researchers have found that drug delivery has as much of an

effect on therapeutic efficacy as does drug potency [28]. Drug delivery can drastically affect a

compound's pharmacokinetics, toxicity, distribution, metabolism, absorption, and cellular uptake,

all of which impact its therapeutic efficacy [29]. As such, biomaterials capable of delivering

therapeutics in a safe and effective manner are necessary to maximize the impact of novel and

existing therapies [29]. Drug delivery systems have been developed to deliver a range of

therapeutics, including genes [30], proteins [31], and small molecule drugs [32]. The necessity

and versatility exhibited by these drug delivery systems has led to much interest in their

development.

2.1. Drug delivery challenges

Despite the benefits that drug delivery systems present, the challenges facing such designs are

myriad. Drug degradation and side effects are primary considerations, and activation of an

immune response must be avoided [29, 33]. In addition, systemic administration of therapeutics

presents the challenges of renal and hepatic clearance, gaining access to the desired

administration site, and removal by the immune system [28, 29, 34]. Local administration of

drugs may not be feasible in certain geometries and can display toxicity due to high drug concentrations [28, 29]. Finally, oral delivery faces the challenges of delivering a functional therapeutic through drastic changes in pH, high concentrations of proteolytic enzymes, and absorption barriers between the oral cavity and bloodstream [28, 29]. Figure 1 displays an overview of the obstacles facing drug delivery systems. While the type of therapeutic and location of delivery will be unique to each application, the aforementioned barriers to drug delivery provide an overview of potential snares to implementation of a drug delivery strategy.
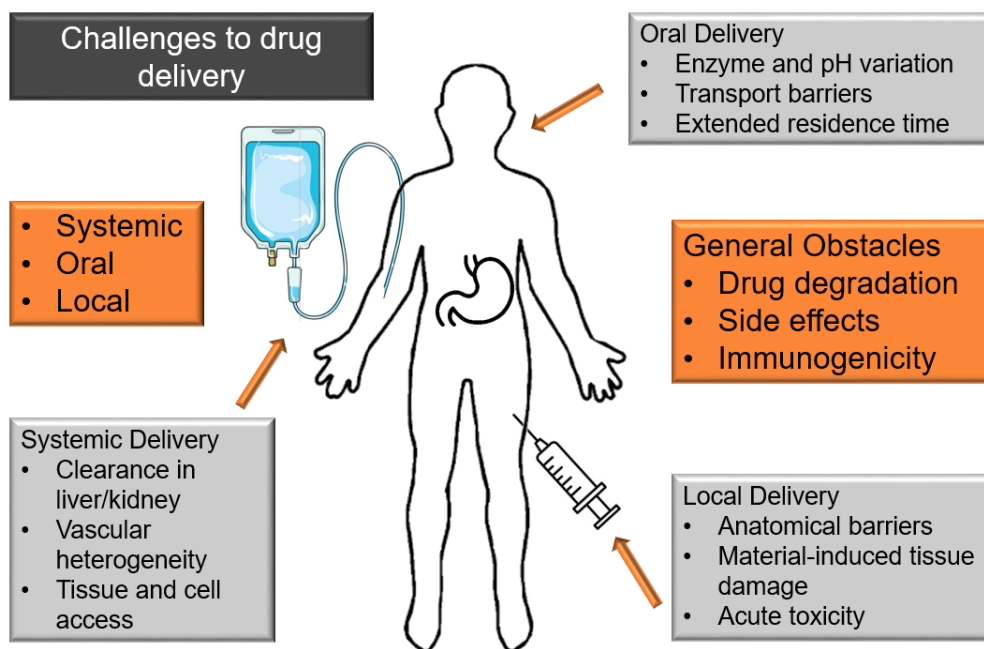
Figure 1: Challenges to drug delivery. Adapted from [29]

2.2. Types of therapeutics delivered

2.2.1. Small molecule drugs

Small molecule drugs, such as the chemotherapy agents doxorubicin (DOX) and paclitaxel (PTX), have frequently been the subject of drug delivery studies [35-39]. Both DOX and PTX are hydrophobic anti-cancer drugs that interact with dividing cells to induce apoptosis [40, 41]. The hydrophobicity of these molecules requires a solubilizing agent for clinical use, but these

solubilizers can cause toxicity and side effects beyond those already associated with the chemotherapy agent [42]. Accordingly, current chemotherapy techniques cause well-known side effects including nausea/vomiting, fatigue, and hair loss [43]. Drug delivery strategies have sought to minimize these adverse effects by solubilizing the active drug in a carrier system capable of transporting it to the cancerous cells and releasing it only where activity is desired. Some studies have formed drug carriers from proteins [44, 45], while others have used liposomes [46], nanoparticles [36, 47], or hydrogels [48-50] to achieve the desired therapeutic effect.

2.2.2. Genes and gene vectors

Gene therapy is a rapidly-growing field in which nucleic acids are altered or transferred to a patient in order to correct genetic diseases, activate immune cells, or induce antibody production [51]. This is accomplished through viral or non-viral gene vectors. Viral vectors seek to take advantage of a virus's natural ability to insert its own nucleic acids into those of the host cell. The most commonly utilized viral vectors include adenovirus, adeno-associated virus, herpes simplex virus, and retrovirus [52-54]. The advantages of this strategy include high infectivity and endosomal escape, prompting numerous groups to develop viral gene vectors for therapeutic use [55].

While the use of viruses for gene delivery presents numerous advantages, viral gene vectors face the challenges of immunogenicity and limited capacity for transgenic material [52]. Accordingly, other studies have developed non-viral vectors for cellular transfection. Positively-charged polymers are common components of non-viral vectors because they enhance cellular uptake through electrostatic interactions with cell membranes [56]. Chitosan, polyethylene imine, and poly(L-lysine) each display cationic properties and have been utilized as the basis for non-viral vectors [57-62].The advantages of non-viral vectors include reduced toxicity and immunogenicity, enhanced versatility, and improved cell specificity, though transfection and

endosomal escape frequently remain obstacles [63]. In response, some have used cationic polymers in conjunction with viruses, which has shown potential to display advantages seen with both the viral and non-viral vectors [62, 64]. With such diversity in design and promise in potential, gene delivery comprises a sizeable portion of all drug delivery investigations.

2.2.3. Therapeutic proteins

Therapeutic proteins make up the remaining category for drug delivery research. Proteins are sequences of amino acids folded into precise conformations and are foundational to most cellular functions [65]. Certain proteins are attractive as therapeutics because they exhibit substrate specificity, catalyze existing biological processes, and are specialized for a single purpose [66, 67]. As with genes and small molecule drugs, the drawbacks of direct administration of therapeutic proteins include both immunogenicity and side effects as well as rapid *in vivo* clearance [67]. This has led numerous groups to investigate drug delivery systems capable of shielding a protein from the immune system while maintaining its medicinal effect. Some architectures explored include protein encapsulation within liposomes [68, 69], hydrogels [70, 71], and nanoparticles [31, 72], while other designs have experimented with direct conjugation between a protein and a hydrophilic polymer [73, 74] (Figure 2).
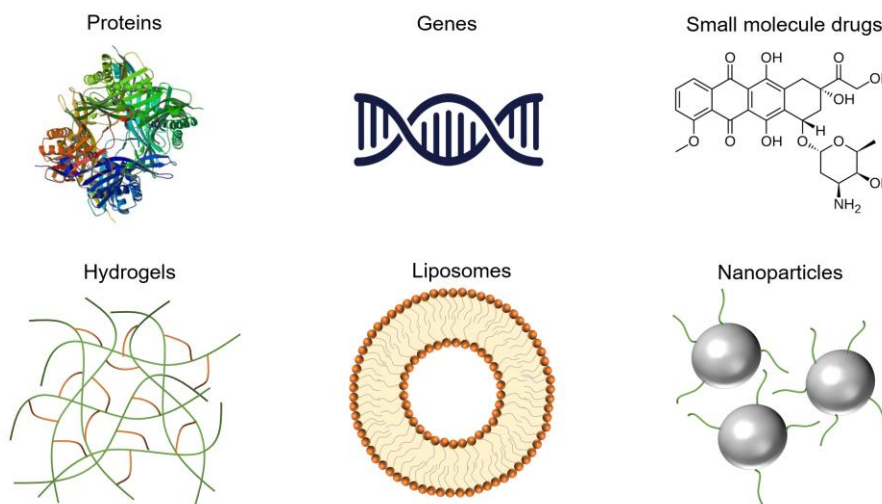
Figure 2: Types of therapeutics and common structures utilized in drug delivery [75]

2.3. Drug delivery strategies

2.3.1. Liposomes

As briefly mentioned, liposomes have been identified as a potential solution to drug delivery challenges. Liposomes are double-layered spheres formed by self-assembly of amphiphilic molecules (molecules containing both polar and non-polar functional groups) [76]. These unique structures shield the liquid entrapped within the inner sphere from the surrounding environment, lending the architecture potential for targeted drug delivery with reduced side effects [77]. While ideal for use with water-soluble small-molecule drugs, liposomes have also been used in protein and gene delivery [69]. Though the exterior of the liposome is already hydrophilic, enhanced liposome stability and retention time has been observed with the inclusion of amphiphilic molecules containing super-hydrophilic polymer conjugates [68]. Furthermore, the encapsulated therapeutic may be selectively released in a targeted environment by variation in pH [78, 79], temperature [80, 81], or the application of ultrasound [82], UV irradiation [83], or a magnetic field [81, 84].

2.3.2. Hydrogels

Drug delivery using hydrogels has been investigated in conjunction with both small-molecule drugs and therapeutic proteins. The solid-phase, hydrated, crosslinked-polymer architecture of hydrogels allows for adsorption, transport, and selective release of a therapeutic [71]. Therapeutics may be either adsorbed within or conjugated to the hydrogel structure for delivery purposes. Several investigations have shown that hydrogels enhance localized delivery of chemotherapy agents and therapeutic proteins through use of stimulus-responsive chemical moieties [48-50, 70, 71, 85, 86]. These moieties have been used to sensitize hydrogels to both endogenous and exogenous stimuli, including pH [48, 87], redox potential [88], and temperature [89].

2.3.3. Nanoparticles

Therapeutic nanoparticles make up the majority of remaining drug delivery strategies. As the term nanoparticle describes anything between 1 nm and 1 μm in diameter, a wide range of materials and compositions have been used to create therapeutic nanoparticles [31, 90, 91]. Broadly speaking, therapeutic nanoparticles can be categorized by their material, with each geometry and architecture providing unique benefits for application-specific particle development.

2.3.3.1. Metal nanoparticles

While metal nanoparticles are utilized in photocatalysis [92], disinfection [93], data storage [94], and magnetic resonance imaging (MRI) [95], metallic nanoparticles also have use in drug delivery applications [96]. Noble metals have been investigated as non-viral gene vectors for their reduced cytotoxicity in comparison to cationic polymers [97]. Another advantage of using metallic components within a nanoparticle is that the electron orbital ordering can impart properties allowing the structure to respond to an applied electromagnetic field or be viewed using MRI or computed tomography (CT) [98-100]. Additionally, metal nanoparticles absorb and scatter light, expanding their function into the area of photodynamic therapy [101].

Metal nanoparticles display unique utility when targeting non-dividing, primary, or stem cells through conjugation with cell-penetrating peptides [97], and may be utilized as components of stimulus-responsive gene delivery systems [102]. Dutta et al. described a system of polymer grafted metal nanoparticles that displayed enhanced release of DOX in acidic conditions [103]. Similarly, Chao et al. presented *in vivo* studies of DOX conjugated metal nanoparticles that showed extended lifespans for tumor-laden mice in comparison to those treated with free DOX [104]. Furthermore, metal nanoparticles have been modified with polymers that allow DNA complexation and confer additional properties to a gene delivery system [105]. With such benefits

and utility, metal nanoparticles continue to be investigated for clinical application of drug delivery.

2.3.3.2. Solid lipid nanoparticles

Solid lipid nanoparticles are nm-scale colloidal dispersions of lipids mixed in water with an emulsifier, making them excellent delivery systems for insoluble small-molecule drugs [106]. Solid lipid nanoparticles have been investigated for applications from oral drug delivery to intradermal delivery using microneedles [107, 108]. Tunable release of loaded drugs has been observed, and modified solid lipid nanoparticles have increased bioavailability of therapeutics in biologically-relevant locations [109]. These systems have been investigated for their ability to encapsulate and release a combination of therapeutics simultaneously while preventing undesirable interactions between the loaded therapeutics [106]. This unique feature of the solid lipid nanoparticle lends it potential to enhance the efficiency of current oral delivery methods.

2.3.3.3. Mesoporous silica nanoparticles

Silica nanoparticles displaying pore diameters between 2 and 50 nm were first recognized as potential drug delivery systems in 2001 [110]. In the past two decades, the mesoporous silica nanoparticle properties of consistent uniform porosity, remarkable surface area (which can exceed 1,000 m^2/g), tunable geometry, and versatility have been applied to numerous drug delivery challenges [111, 112]. The drug release profile can be tuned using chemical gates to cover the pore openings of the nanoparticle until a stimulus triggers the release of the entrapped cargo [112, 113]. Furthermore, silanol functional groups on the surface of silica nanoparticles have been shown to stimulate tissue regeneration [114] and can be chemically modified to attach additional functional groups to the nanoparticle [111, 115, 116]. Mesoporous silica nanoparticles can be utilized in conjunction with other drug delivery strategies as well; silica nanoparticles have formed the basis for redox-responsive nanocarriers [116], have been used in magnetically

targeted gene delivery [115], and have been used to solubilize and deliver chemotherapy agents [117]. Such advantages of mesoporous silica nanoparticles suggest continued development as drug delivery systems in upcoming years.

2.3.3.4. Polymer nanoparticles

Polymer nanoparticles make up the majority of remaining drug delivery strategies. As expressed previously, polymers are frequently utilized as add-ons to other drug delivery architectures. Furthermore, polymers have been utilized as the primary components of nanoparticles designed to deliver therapeutics to diverse areas including eyes [118, 119], lungs [120], and tumors [121, 122]. Polymers displaying differing properties are frequently combined into grafted or block copolymers exhibiting the properties of the constituent polymers [123-125]. The functionality of these copolymers can vary widely, from conferring a nanoparticle with stimulus-responsive properties to extending its *in vivo* circulation time through reduced non-specific protein adsorption [68, 126]. This versatility has resulted in polymer and copolymer nanoparticles delivering a range of therapeutics to drastically varying environments [31, 36, 47, 57-62, 72].

2.4. Surface modifications

One recurring challenge that all macromolecular drug delivery systems face is recognition and elimination by the immune system. *In vivo*, a corona of serum proteins becomes adsorbed to the surface of nanoscale delivery systems [127, 128]. This protein corona directly influences the biological fate of a nanoscale drug delivery system, from rapid removal by the immune system to extended residence within the circulatory system [129]. Adsorbed opsonins mark a nanoparticle for phagocytosis, whereas clusterins actually improve the longevity of nanoparticles *in vivo* [130, 131]. Researchers have developed methods to control the composition of the protein corona, and in doing so have been able to control the fate of nanotherapeutics [132]. This is frequently accomplished with the help of hydrophilic polymers, which have long been known to reduce non-

specific protein adsorption, but have more recently been recognized for enhancing adsorption of specific "stealth" proteins [2, 132].

Poly(ethylene glycol) (PEG) is ubiquitous in drug delivery applications for its ability to reduce immunogenicity of therapeutics. PEG and other hydrophilic polymers form a hydration layer by arranging the surrounding water molecules into an ordered structure [133, 134]. This long-range order creates an energy barrier that must be overcome to contact the polymer [134, 135]. For this reason, PEGylation is used to confer biocompatibility to nanoscale drug delivery systems in a variety of ways, from direct protein conjugation to modification of non-viral gene vectors [136, 137]. Additionally, PEG has been shown to selectively adsorb clusterin and apolipoprotein A-I, which have been shown to reduce non-specific cellular uptake [132]. This understanding of the PEG mechanism allows for more effective nanoparticle design.

PEG does exhibit several drawbacks. PEGylation may decrease the bioactivity or efficacy of a therapeutic [138]. More concerning, however, is that continued administration of PEGylated proteins has been shown to induce production of anti-PEG antibodies [139, 140]. With these issues confronting PEG, alternative biocompatible coatings have been investigated. Zwitterions, neutrally charged compounds that contain at least one positive and one negative charge, have displayed an even greater ability to resist non-specific protein adsorption than PEG [134]. Several types of zwitterions have been polymerized and are currently being utilized in drug delivery systems to overcome the challenges associated with PEG immunogenicity [26, 36, 141-145]. Poly(carboxybetaine) and poly(sulfobetaine) have been shown to enhance the circulation time of conjugated therapeutics [146-164], whereas poly(phosphorylcholine) displays strong cellular uptake properties [133, 165-170]. Consequently, zwitterionic polymers show potential as a PEG alternative to reduce non-specific protein adsorption in nanotherapeutics.

2.5. Targeting/stimulus-responsive moieties

2.5.1. Targeted drug delivery

Targeted drug delivery seeks to increase the relative concentration of a therapeutic in a medicinally-relevant environment in comparison to the surrounding tissue in order to enhance therapeutic efficacy and reduce side effects [34]. In general, targeting strategies can be divided into passive targeting, in which properties of the therapeutic and targeted environment work together to enhance the local therapeutic concentration, and active targeting, in which targeting moieties are attached to the surface of a drug delivery system [171, 172]. The simplest passive targeting strategy relies on the enhanced permeability and retention (EPR) effect. The rapid growth of cancerous tissue creates a disorganized network of neovascularization containing expanded gap junctions and increased lymphatic drainage [173]. This leaky vasculature promotes a passive buildup of nanoparticles larger than 50 kDA within the tumor [173-175]. Several delivery vehicles utilize the EPR effect to passively target a tumor before reduced pH or elevated redox potential stimulates drug release [36, 37, 58, 142, 176-180].

While the EPR effect is a useful passive targeting mechanism, some systems integrate active targeting for drug delivery. One system known as antibody targeted, triggered, electrically modified prodrug-type strategy (ATTEMPTS) utilized antibody targeting of an inactive drug and therapeutic activation through a subsequently dosed protein [181-184]. Other nanoparticles have been conjugated with peptide sequences that selectively bind to receptors upregulated in the targeted environment, such as the folate receptor in certain cancers [185-187]. These surface modifications, along with selective small molecules and aptamers, allow targeting optimization through variation in the method and density of conjugation [188]. Consequently, targeting moieties can enhance the efficacy and reduce the side effects of drug delivery systems.

2.5.2. Exogenous stimuli for drug release

As briefly discussed, drug delivery systems have been designed to respond to exogenous stimuli. Much recent progress has been made in the field of photodynamic therapy, in which inactive compounds are made therapeutically relevant upon photoactivation [189]. Chen et al. employed this strategy for cancer treatment. Photosensitive compounds were loaded into nanocarriers and accumulated in tumor regions through the EPR effect before photoirradiation generated ROS and damaged the cancer cells [101, 189]. This cytotoxic effect was localized to the tumor due to the short ROS half-life, which prevented damage beyond the irradiated area.[189]

Ultrasound-responsive drug delivery systems work in a similar fashion. Ultrasound can induce cavitation-effected drug release from microbubbles, allowing for a therapeutic to remain inactive until activated by exogenous ultrasound [190]. This technique has been utilized for delivering therapeutics across the blood brain barrier, a particularly challenging drug delivery target [191, 192]. Application of ultrasound can also enhance nanoparticle transport properties for ocular drug delivery [22]. The properties of ultrasound as a drug delivery and release mechanism lend it credence for continued therapeutic use.

Application of an external electromagnetic field has been used widely for both drug delivery and theranostics, in which diagnosis and treatment are carried out simultaneously [193]. Magnetic nanoparticles can be observed with MRI, which allows for therapeutic delivery with high spacial-temporal resolution [194, 195]. For pure delivery applications, metal nanoparticles exhibiting superparamagnetism can be drawn to the desired area of effect using a magnetic field [196]. Superparamagnetic properties are displayed in metal nanoparticles below 10 nm in diameter, thus conferring exogenous targeting capabilities to any structure of which they are a constituent [96, 196]. This form of external control is useful for treating hypoxic tumors, which are difficult to target using conventional chemotherapy techniques due to reduced circulation [196, 197].

Finally, temperature can be harnessed as an exogenous stimulus for drug delivery. Several polymers display changes in conformation or solubility with varying temperature [89, 103, 198-201]. Thermo-responsive drug delivery architectures capitalize on these properties to release loaded therapeutics at elevated temperatures [103, 200, 202]. One fascinating study developed an amphiphilic block copolymer in which one block displayed an upper critical solubility temperature (UCST) and another showed a lower critical solubility temperature (LCST) to form colloidal associations [203]. The UCST and LCST were tuned such that a transition in temperature reversed the solubility and thus the orientation of the colloidal subunits to release an entrapped therapeutic [203]. Consequently, temperature variations have been shown to be another effective alternative for exogenous triggering of drug release.

2.5.3. Endogenous stimuli for drug release

Other designs have sought to capitalize on variations in the microenvironment where drug release is desired. Common endogenous stimuli include variations in pH, increased redox potential, and elevated concentrations of ROS, which are all characteristics exhibited by cancers [204, 205]. Nanocarriers have shown enhanced therapeutic efficacy in these conditions through variation in structure swelling, surface charge transition, or bond degradation that releases a therapeutic or enhances cellular uptake [58, 142, 176-179].

pH-sensitivity can be attained in several ways. Hydrozone linkages are pH-responsive and constitute one method to selectively release a therapeutic in an acidic environment [206]. For example, Chen et al. incorporated hydrozone linkages in polymer-DOX prodrugs. DOX release increased in acidic conditions, and cell-culture studies showed that a maximum tolerated DOX dose (MTD) was 3 to 5 times greater than the MTD of free DOX [142, 178]. Additionally, polymers can exhibit unique pH-dependent properties based on variations in swelling; DOX has been loaded into hydrogels that take a condensed configuration at pH 7.4 but expand in acidic

conditions [48, 87]. Finally, some polymers display pH-sensitivity based on the pKa of their constituent ions, which confers them with unique drug delivery properties [207]. Enhanced therapeutic efficacy in a tumor can be achieved utilizing a pH-triggered mechanism to induce a change in ζ-potential from negative to positive, which can enhance cellular uptake by improving binding efficacy to negatively charged cellular membranes [58, 176]. Ou et al. developed one such system with phosphorylcholine-based micelles that demonstrated an increase in cellular uptake in an acidic environment prompted by a change in surface charge [176].

Both redox- and ROS-responsive drug delivery systems seek to take advantage of the enhanced oxidative stress common to cancer cells. Continuous cellular replication necessarily increases the concentration of ROS and glutathione (GSH), the cellular redox regulator, within the tumor region [208-210]. ROS-responsive gene delivery systems have been designed to exhibit a ζ-potential change in the presence of peroxide. Recently, Li et al. developed a ROS-responsive dendrimer that exhibited a ζ-potential shift when exposed to 80 mM H_2O_2 and resulted in a transfection efficiency 4.5 times higher than PEI [179]. ROS sensitivity can also be attained by including a thioketal-containing linker, which degrades in response to elevated ROS and allows for highly specific drug release profiles [211].

Redox-responsive drug delivery systems rely on the reduction of disulfide bonds incorporated into the delivery system structure to release an encapsulated cargo [88, 212, 213]. Disulfide linkages have been incorporated into all varieties of drug delivery systems and have been used to deliver proteins as well as genes and small molecule drugs [180]. To improve cancer targeting, some have created dual-stimuli-responsive nanoparticles that respond to both elevated ROS and GSH, allowing for further enhanced drug delivery efficacy [20, 213, 214]. Consequently, redox-responsive drug delivery systems may show therapeutic encapsulation and retention in circulation before disulfide reduction releases the active compound in a reductive environment. Figure 3

summarizes some targeting strategies and stimuli utilized to trigger drug release from drug delivery systems.
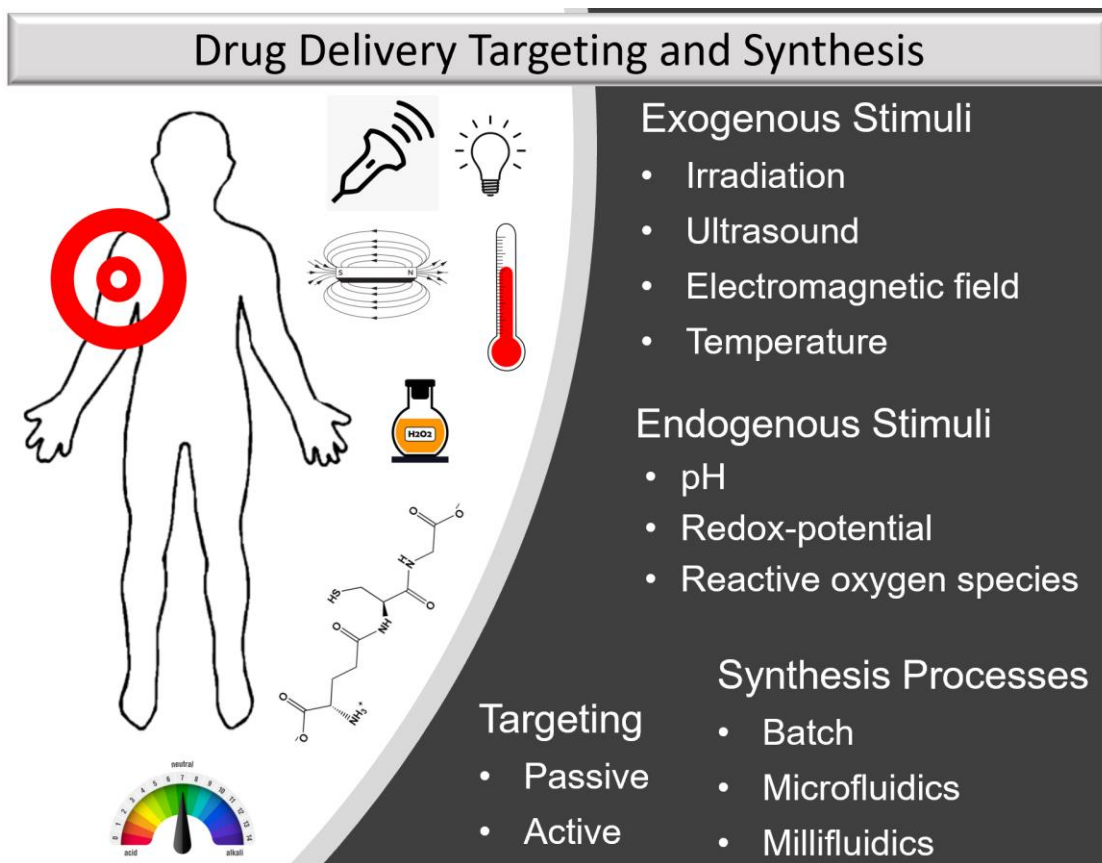
Figure 3: Targeting strategies and stimuli for drug delivery systems

2.6. Synthesis methods for nanoparticle drug delivery systems

The size, distribution, and stability that nanoparticles exhibit have been linked to the processes by which they are formed [215-217]. Most nanoparticles are formed in batch processes through a process such as nanoprecipitation or self-assembly [218]. While batch processes are a simple and practical strategy for nanoparticle development, their discontinuous nature offers few factors for tuning and presents challenges in controlling nanoparticle size and distribution [23, 219]. Batch processes can also suffer from batch-to-batch variation, which can limit consistency and reproducibility [217].

Continuous flow systems show potential to overcome these limitations [219]. Microfluidics have been proposed as a more efficient alternative for the preparation of monodisperse nanoparticles with tunable properties [220]. Microfluidics provide tunable and homogeneous synthesis environments that can be monitored at microscale to control the biological properties of the nanoparticles [221, 222]. Additional benefits include reproducibility, simplicity, cost-effectiveness, and enhanced safety; such characteristics have made microfluidics the subject of investigation for nanoparticle synthesis with a variety of materials [223, 224].

Similarly, millifluidic configurations display the advantages of microfluidics while also boasting reduced cost and enhanced process control through simple determination of flow rates and residence times [219, 225]. Furthermore, millifluidics are more resistant to fouling than microfluidics and can more easily provide an isothermal and homogeneous synthesis environment [220, 226]. Until now, millifluidics have been primarily used in the synthesis of inorganic and metal nanostructures, whereas millifluidic synthesis of organic nanoparticles has been limited [227, 228]. When utilized, millifluidic synthesis has proved successful; Libi et al. synthesized poly(lactide co-glycolic) acid (PLGA) nanoparticles using a millifluidic configuration to produce nanoparticle diameters ranging from 220 to 250 nm [225]. In the study, a minimum particle size of 196.93 ± 14.30 nm was achieved using the millifluidic configuration, which was close to the value attained by the batch process (198.43 ± 0.95 nm) [225].

Millifluidic synthesis processes have also been used to better control sizes of drug nanocomplexes. Tran et al. developed a millifluidic synthesis platform capable of tuning curcumin/chitosan nanoparticle size by controlling the residence time [23]. Curcumin nanoplexes synthesized with millifluidics displayed a ζ-potential of +15 mV, a 72 wt% drug payload, and a diameter of 115 nm, a six-fold size decrease over the bulk mixing synthesis method [23]. Similarly, Dong and Hadinoto performed a direct comparison between a millifluidic process and a bulk mixing process to create perphenazine/dextran sulfate nanoplexes [220]. Both the batch

and the continuous processes produced 70-90 nm particles with ζ-potential approaching -50 mV, but the millifluidic nanocomplex exhibited a 31% higher drug loading than the nanocomplex formed through the batch process [220].

Both microfluidic and millifluidic processes suffer from a lack of mixing. At such length scales, Reynolds numbers do not approach that required for transition flow, resulting in limited mass transfer [216]. Consequently, methods have been developed to enhance diffusion in a laminar flow regime through passive and active mixers [215]. Passive mixers redesign the flow channel to reduce the diffusion length, but these are susceptible to fouling and are challenging to manufacture on µm-scales [215, 229]. Alternatively, active mixers enhance diffusion without channel modification through the application of electromagnetic or acoustic energy [215, 230]. Acoustic energy input has been shown to produce cavitation, and the interactions between vapor bubbles and the remaining liquid solvent enhances molecular diffusion [230]. Therefore, each continuous micro- or millifluidic nanoparticle synthesis process must address this challenge of mixing before nanoparticles can be produced.

Ultrasonication has been used to enhance diffusion in the synthesis of inorganic nanoparticles in millifluidic processes [231-237]. Furthermore, ultrasound has been shown to reduce fouling and induce uniform mixing in small-scale flow processes through cavitation [237, 238]. Ultrasound with frequencies ranging between 20 kHz and 1 MHz creates cavitation micro-bubbles with diameters on the same order of magnitude as millifluidic channels, which can increase the cavitation mixing effect through resonance [237, 239, 240]. With such evidence for ultrasound enhancing previous millifluidic processes, application of ultrasound to the synthesis of therapeutic nanoparticles holds potential for repeatable, controlled mixing in laminar flow regimes.

2.7. Conclusions

The challenges of drug delivery are difficult to overcome, but numerous strategies exist to surmount the side effects, low circulation time, poor bioavailability, and reduced cellular uptake associated with many therapeutics. Each application requires unique properties from a delivery device, which has led to the development of diverse drug delivery systems. Drug delivery will continue to expand through the discovery of novel biomaterials and the combination of existing materials in novel configurations. Furthermore, rapid synthesis of clinical therapeutics will be required as an increasing number of drug delivery systems gain FDA approval. The discovery of translational medicines is crucial, and the field of therapeutic drug delivery is expected to continue its rapid growth in the approaching decades.

CHAPTER III

EFFECT OF REDOX-RESPONSIVE DTSSP CROSSLINKING ON POLY(L-LYSINE)-
GRAFTED-POLY(ETHYLENE GLYCOL) NANOPARTICLES FOR DELIVERY OF
PROTEINS

3.1. Introduction

Therapeutic proteins are widely recognized for their utility in treating a number of diseases, including pulmonary embolism, cancer, diabetes, and arthritis [1, 2]. Despite this efficacy, systemic administration of therapeutic proteins faces hurdles including side effects and rapid *in vivo* clearance [67]. A common approach toward overcoming these challenges is to use biocompatible polymers to shield proteins from identification and elimination by the immune system [8]. Much recent interest has been paid to investigating benefits of polymeric nanoparticles in protein delivery.

One advantage of utilizing polymeric materials to encapsulate proteins is that stimulus-responsive moieties can be included within the polymer structure. These moieties undergo a conformational change or induce particle destabilization leading to protein release in response to localized environmental conditions [16]. The development of such materials is of considerable interest, as this strategy enhances the efficacy of protein therapy by minimizing side effects and reducing immunogenicity while retaining protein function in a desired region. Common endogenous

triggers include pH [18-21, 241], redox potential [19, 20, 242], or presence of reactive oxygen species [243], whereas exogenous triggers include temperature [244, 245], magnetic field [246], irradiation [247-251], ultrasound [22, 191], and subsequently dosed protein triggers [182, 252].

Glutathione (GSH) is a tripeptide that plays a central role in the maintenance of cellular reduction potential [209, 253]. When a cell is under enhanced oxidative stress, elevated GSH concentrations are required to maintain homeostasis [209, 254]. Abnormal GSH levels are characteristic of various types of cancer, including brain tumors [255], breast cancers [208, 256-258], prostate cancers [259, 260], and lung cancers [256, 261]. Consequently, numerous drug delivery systems have been designed to release a drug when exposed to atypical GSH concentrations [262-268].

Polymeric nanoparticles have been developed to respond to increased reduction potential with a solubility shift [269], topology change [270], or core-shell separation [271], but no studies have investigated how redox-responsive crosslinking affects the properties of self-assembled copolymer-protein nanoparticles. Previously, poly(L-lysine) was grafted with poly(ethylene glycol) (PLL-g-PEG) and used to encapsulate a model protein via an electrostatic self-assembly mechanism [26]; the current study sought to understand how redox-responsive crosslinking may alter the nanoparticle size, dispersity, and stability. 3,3'-dithiobis(sulfosuccinimidyl propionate) (DTSSP) was utilized as an amine-reactive redox-responsive crosslinker, as it contains a disulfide to enable selective nanoparticle destabilization and protein release. Bovine serum albumin, selected for its stability, was encapsulated within PLL-g-PEG to create a library of crosslinked polymer-protein nanoparticles (DTSSP NPs). All DTSSP NPs were characterized by size, polydispersity index, and encapsulation efficiency. Subsequently, DTSSP NPs displaying the best combination of size and encapsulation efficiency were further characterized by retention of encapsulated protein activity, stability in the presence of serum and proteases, and crosslinking destabilization in a reductive environment.

3.2. Materials and methods

Lyophilized bovine serum albumin (BSA), fetal bovine serum (FBS), α-chymotrypsin from bovine pancreas, sodium dodecyl sulfate (≥98.5%, SDS), and poly(L-lysine)-HBr (PLL-HBr) with molecular weight 15-30 kDa were purchased from Sigma Aldrich (St. Louis, MO). Poly(ethylene glycol) of 5 kDa molecular weight and functionalized with a carboxymethyl succinimidyl ester (mPEG-NHS) was purchased from Creative PEGworks (Durham, NC). Dimethyl sulfoxide (DMSO), 3,3'-dithiobis(sulfosuccinimidyl propionate) (DTSSP), disuccinimidyl suberate (DSS), dithiothreitol (DTT), heparin sodium salt (13.5 kDa MW), p-nitrophenyl acetate (NPA), 4-nitrophenol, acrylamide/bisacrylamide (37.5:1) and other polyacrylamide gel casting and running materials were purchased from Fisher Scientific (Pittsburgh, PA). DQ Green BSA was purchased from Life Technologies (Grand Island, NY). Phosphate buffer saline (PBS, pH 7.4, 10 mM) was made in-house.
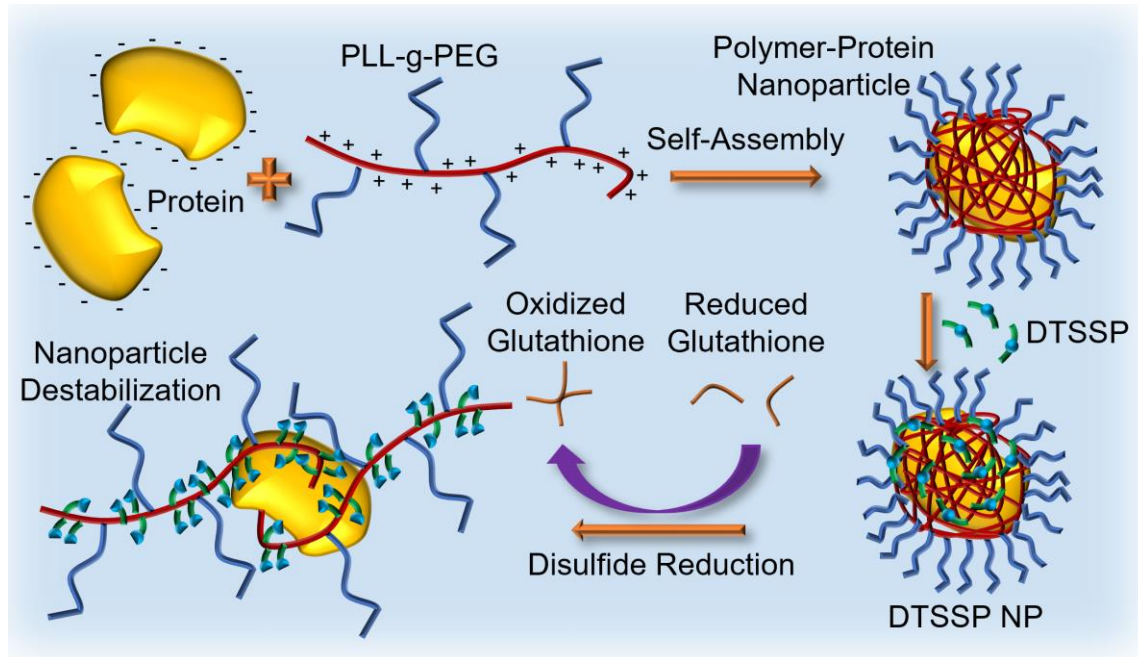
Figure 4: Assembly and destabilization of polymer-protein nanoparticles crosslinked with DTSSP. mPEG-NHS (5 kDa) was grafted onto 11% of the lysine residues on 15-30 kDa PLL-

HBr to create PLL-g-PEG. Electrostatic self-assembly was accomplished by encapsulating bovine serum albumin in varying ratios of PLL-g-PEG and create polymer-protein nanoparticles. The nanoparticles were subsequently crosslinked with varying concentrations of DTSSP, which contains a disulfide reducible by glutathione, to create a library of DTSSP NPs. Exposure to glutathione reduces the disulfide crosslinking, destabilizing the DTSSP NP structure and exposing the protein to the environment.

3.2.1. PLL-g-PEG copolymer synthesis

PLL-g-PEG was synthesized according to the methods described by Flynn et al. [26], in which succinimidyl ester functional groups on mPEG-NHS were reacted with primary amines on PLL-HBr. A PLL solution containing 15 mg of PLL-HBr in 200 μL PBS was created, and 57 mg of 5 kDa mPEG-NHS were subsequently added for a desired 10% PEG grafting ratio. These molecular weights and grafting ratio were selected such that the PEG would take the brush conformation and extend the circulation time of the copolymer nanoparticle without greatly increasing its size [26, 272]. The PLL-g-PEG solution was incubated at 25°C for 2 hours before being washed three times with 300 μL ultrapure water using a Pierce™ Protein Concentrator with a 10 kDa molecular weight cutoff (MWCO) (ThermoFisher Scientific, Waltham, MA). After washing, four samples were combined, diluted to 1 mL in ultrapure water, and stored overnight at -80°C. After freezing, the copolymer was removed from -80°C storage and freeze-dried for 24 hours. The lyophilized copolymer was stored at -20°C until use. The achieved grafting ratio of PEG to PLL was determined through ^{1}H NMR spectroscopy.

3.2.2. Synthesis of the nanoparticle library

DTSSP NPs were formed based on the procedure described by Flynn et al. [26]. BSA solution was made by adding 2.0 mg lyophilized BSA to 1.0 mL PBS and allowing the protein to dissolve for 30 minutes. The BSA solution was then filtered through a 0.20 μm syringe filter to remove

large aggregates, and the absorbance at 280 nm was used to determine the concentration. The

BSA solution was then diluted to 0.27 mg/mL in PBS. Lyophilized PLL-g-PEG was dissolved in

PBS to 6, 10, and 15 mg/mL, and 7.5 μL PLL-g-PEG solution were added to 25 μL BSA solution

under gentle vortexing to create nanoparticles with copolymer to protein mass ratios of 7:1, 11:1,

and 17:1. The polymer-protein nanoparticles were incubated at 25°C for 30 minutes to allow

electrostatic self-assembly. Once assembled, the nanoparticles were crosslinked with the amine-

reactive crosslinker 3,3'-dithiobis(sulfosuccinimidyl propionate) (DTSSP), which is made up of

sulfonated NHS-ester terminal groups with a central reducible disulfide bond along a 12 Å spacer

arm. DTSSP was dissolved in PBS to 0.25, 2.5, 10, and 25 mg/mL, and 5 μL were added under

gentle vortexing to the self-assembled nanoparticles to create DTSSP NPs with crosslinker to

protein mass ratios of 0.2:1, 2:1, 8:1, and 20:1. The DTSSP NPs were incubated at 25°C for 1

hour and used immediately or stored at 4°C.

3.2.3. Nanoparticle size and ζ-potential measurement

DTSSP NP hydrodynamic diameters were measured using a ZetaPALS ζ-potential analyzer

(Brookhaven Instruments Corporation, Holtsville, NY). DTSSP NP samples were diluted in PBS

to 50 μL and loaded into a disposable microcuvette. Five measurements, each lasting 30 seconds

and measured at a 90° angle, were used to determine the hydrodynamic diameter of the DTSSP

NPs through dynamic light scattering (DLS). DTSSP NP ζ-potential was measured using the

same instrument through phase analysis light scattering and the Smoluchowski equation. Five

batches of 10x by volume DTSSP NPs were combined and loaded into a disposable cuvette, and

30 converged measurements were used to determine the average ζ-potential.

3.2.4. Gel migration assay for protein encapsulation

The DTSSP NP protein encapsulation efficiency was measured using a non-reducing gel

migration assay. DTSSP NP samples were completed to 37.5 μL with PBS and subsequently

diluted with 37.5 µL non-reducing SDS-PAGE sample buffer. Samples were not boiled but were incubated at 37°C and shaken on a ThermoFisher Max400Q orbital shaker (Thermofisher, Waltham, MA) at 80 rpm for 15 minutes before 27 µL of each sample were added to an 8% SDS-PAGE gel. SDS-PAGE gels were run at 200 V on a Bio-Rad Tetracell mini gel electrophoresis apparatus (Bio-Rad Laboratories, Hercules, CA) until the dye front reached the bottom of the gel (approximately 45 minutes). The running buffer did not contain SDS. SDS-PAGE gels were stained with Coomassie G-250 before imaging. The extent of protein encapsulation within the DTSSP NPs was determined relative to the band intensity of free BSA, and ImageJ analysis was used to quantify encapsulation by integrating the BSA monomer peak between the local minima. After encapsulation studies were completed, one DTSSP NP composition was selected for further characterization to reduce the required number of experiments.

3.2.5. Scanning electron microscopy analysis of nanoparticles

The DTSSP NP size distribution was observed using an FEI Quanta™ 600 scanning electron microscope (ThermoFisher, Waltham, MA). DTSSP NPs were synthesized and transferred from PBS to ultrapure water using a Pierce™ Protein Concentrator with a 10 kDa MWCO. Aluminum scanning electron microscopy (SEM) stubs were drop cast with 20 µL of DTSSP NPs and were dried at room temperature for 20 hours. The dried samples were sputter-coated with gold-palladium using a Cressington 108 sputter coater (Cressington Scientific Instruments, Watford, England). Images were recorded at an accelerating voltage of 20.0 kV, and DTSSP NP size distribution was determined from 151 particles using ImageJ analysis. The size distribution was used to estimate the concentration and loading of the DTSSP NPs assuming smooth sphere geometry, a 7:1 C:P volume ratio, and a BSA geometry of 4 nm by 4 nm by 14 nm [273].

3.2.6. Transmission electron microscopy analysis of nanoparticles

Nanoparticle size and morphology were analyzed using transmission electron microscopy (TEM). DTSSP NPs were synthesized and transferred to ultrapure water using a Pierce™ Protein Concentrator with a 10 kDa MWCO. A graphene-oxide TEM grid was deposited with 10 μL of DTSSP NPs and dried at room temperature for 30 minutes. The sample was observed using a JEOL JEM-2100 electron microscope (JEOL Ltd., Akishima, Tokyo, Japan) with an accelerating voltage of 200 kV.

3.2.7. Retention of esterolytic activity

To determine the effect of encapsulation on the activity of the encapsulated protein, DTSSP NPs were incubated with p-nitrophenyl acetate (NPA). While previously disputed, it has been shown that BSA exhibits mild esterolytic activity around active site Tyr411 [274]. Esterolytic breakdown of NPA produces 4-nitrophenol, which displays an absorption peak at 410 nm and allows the product concentration to be monitored spectrophotometrically [275]. Samples of BSA, PLL-g-PEG, PLL-g-PEG crosslinked with DTSSP, Non-X NPs, and DTSSP NPs were diluted to 100 μL in PBS and 80 μL were loaded onto a 96 well plate (Corning Inc., Corning, NY). Once loaded, 30 μL of 8.7 mM NPA in isopropyl alcohol was added to each well for a final concentration of 2.4 mM. The plate was incubated at 37°C with absorbance at 410 nm measured in 10-minute increments using a Packard Spectracount plate reader (Cole-Palmer, Vernon Hills, IL). The concentration of 4-nitrophenol was determined from a standard curve, and the concentration of 4-nitrophenol from NPA in PBS was subtracted from the samples to control for substrate hydrolysis.

3.2.8. Nanoparticle stability

Nanoparticle stability in the presence of serum, polyanions, and proteases, as well as destabilization and protein release in a reductive environment were measured using fluorescence assays. Unlike the BSA used in the preceding experiments, DQ Green BSA (DQBSA) was utilized as the encapsulated model protein. DQBSA is BSA so heavily haptenated with 4,4-difluoro-5,7-dimethyl-4-bora-3a,4a-diaza-s-indacene-3-propionic acid fluorophore (BODIPY FL) that it experiences self-quenching relievable through protein denaturation [276]. When incubated with either SDS or proteases, free DQBSA displays a sharp increase in fluorescence while DQBSA that remains encapsulated within the copolymer retains its initial fluorescence, allowing for relative encapsulation to be quantified.

3.2.8.1. Nanoparticle stability in the presence of polyanions

A fluorescence assay was used to determine the stability of DTSSP NPs in the presence of heparin, a naturally-produced sulfated glycosaminoglycan with the highest negative charge density of any known biomolecule.[277, 278] DTSSP NPs were synthesized with DQBSA and incubated with 0.27 mM heparin in PBS for 1 hour. DTSSP NPs were diluted with 200 μL PBS and aliquots of 100 μL were loaded onto a 96 well plate. The fluorescence was measured (485 nm excitation, 535 nm emission) using a Beckman Coulter DTX 880 Multimode Detector (Beckman Coulter Life Sciences, Brea, CA) before and after addition of 20 μL 10% SDS to each well, which denatured any unencapsulated protein.

3.2.8.2. Nanoparticle stability in serum

Nanoparticle stability in serum was measured using a fluorescence assay. DTSSP NPs were synthesized with DQBSA, diluted to 200 μL in FBS (5, 10, and 25 vol%) and make-up PBS, and incubated at 37°C. After 22 hours, 100 μL aliquots of 10% SDS were added to DTSSP NP

samples, and the samples were loaded onto a 96 well plate. The plate was read with a DTX 880 Multimode Detector at 485 nm excitation and 535 nm emission.

3.2.8.3. Nanoparticle stability in the presence of proteases

The ability of the DTSSP NPs to protect the encapsulated protein from protease degradation was measured using a fluorescence assay. DTSSP NPs were synthesized, diluted in PBS to 340 µL, and 100 µL aliquots were loaded onto a 96 well plate. α-Chymotrypsin from bovine pancreas was dissolved in PBS (0.6 mg/mL) and 20 µL were added to wells containing free DQBSA, Non-X NPs, DTSSP NPs, and nanoparticles crosslinked with a non-reducible DTSSP analog, disuccinimidyl suberate (DSS NPs). Plate fluorescence was read immediately and periodically afterwards with a DTX 880 Multimode Detector at 485 nm excitation and 535 nm emission. The plate was incubated between measurements at 37°C on a Max400Q orbital shaker operating at 50 rpm.

3.2.9. Nanoparticle destabilization in a reductive environment

Destabilization of DTSSP NPs in a reductive environment was measured using a fluorescence assay. Free DQBSA, DTSSP NPs, and DSS NPs were synthesized, diluted with 600 µL PBS, and 100 µL aliquots were loaded onto a 96 well plate. The fluorescence was measured initially at 485 nm excitation, 535 nm emission using a DTX 880 Multimode Detector before each well was diluted with 30 µL 10 wt% SDS. The fluorescence was measured again, and 10 µL of either PBS or DTT (final concentrations of 0.20, 1.0, and 5.0 mM) were subsequently added to each well. The plate was incubated at 37°C and 30 rpm on a Max400Q orbital shaker with fluorescence measured periodically after initial DTT addition. The protein release profile in varying DTT concentrations was calculated by normalizing the DTSSP NP fluorescence in the presence of DTT with reference to the fluorescence displayed by free DQBSA in DTT and the DTSSP NP in the presence of PBS.

3.2.10. Statistical analysis

Statistical analysis was performed in Microsoft Excel using a two-tailed heteroscedastic student's *t*-test. A minimum of 3 samples were used for each measurement.

3.3. Results and discussion

3.3.1. Effect of DTSSP crosslinking on nanoparticle size and encapsulation

The achieved grafting of PEG to PLL was determined from the ^{1}H NMR spectra and found to be 11%. Nanoparticle sizes varied based on the copolymer to protein (C:P) and the crosslinker to protein (X:P) mass ratios as shown in Table 1. At the 7:1 C:P ratio, DTSSP NP diameter increased linearly with increasing X:P ratio from 13.4 nm to 48.2 nm. In contrast, the diameters at the 11:1 C:P ratio did not display a trend with varying crosslinker concentration, but instead showed a particle diameter of 2.5 µm at a 2:1 X:P ratio. The DTSSP NPs made with the 17:1 C:P ratio were larger than the DTSSP NPs synthesized with the 7:1 C:P at all crosslinker concentrations and generally displayed decreasing diameter with increasing X:P ratio. Furthermore, the diameter of the DTSSP NPs synthesized at the 17:1 C:P and the 0.2:1 X:P ratio matched that of the 2.5 µm observed at the 11:1 C:P and 2:1 X:P ratios. These were the largest particle sizes observed, and the diameter displayed sharp decreases with variation in either X:P ratio or C:P ratio. At the 8:1 and 20:1 X:P ratios, DTSSP NP diameters varied little with C:P ratio and were less than 50 nm at all C:P ratios tested.

The polydispersity index (PDI) of the DTSSP NPs was generally larger at lower X:P ratios and decreased with increasing X:P ratio. With the 7:1 C:P ratio, the PDI began at 0.33 with no DTSSP, peaked at 0.39 for the 2:1 X:P ratio, and decreased to 0.18 at the 20:1 X:P ratio. The 11:1 C:P ratio displayed an initial PDI of 0.23 with no DTSSP, but spiked to 0.576 with the 0.2:1 X:P ratio before decreasing to 0.19 for the 20:1 X:P ratio. The 17:1 C:P ratio showed an initial PDI of

0.28 before decreasing to 0.19 at the 20:1 X:P ratio. These measurements indicate that PDI became independent of the C:P ratio as the X:P ratio increased.

Table 1: Dynamic light scattering (DLS) results for nanoparticles of poly(L-lysine)-grafted-poly(ethylene glycol) encapsulating bovine serum albumin and crosslinked with DTSSP (DTSSP NPs). DTSSP NP hydrodynamic diameters and polydispersity index (PDI) varied with copolymer to protein (C:P) and crosslinker to protein (X:P) mass ratios. Free BSA displayed a diameter of approximately 8 nm.

Diameter (nm)	7:1 C:P Ratio		11:1 C:P Ratio		17:1 C:P Ratio	
X:P Ratio	Average	SD	Average	SD	Average	SD
No DTSSP	13.4	0.40	59.7	18.4	29.9	2.90
0.2:1	18.2	0.70	33.3	11.6	2,530	1,470
2:1	23.5	2.96	2,530	1,420	85.6	28.9
8:1	37.3	4.57	33.0	10.4	49.7	1.80
20:1	48.2	9.06	41.9	0.90	48.4	0.80

PDI	7:1 C:P Ratio		11:1 C:P Ratio		17:1 C:P Ratio	
X:P Ratio	Average	SD	Average	SD	Average	SD
No DTSSP	0.331	0.055	0.225	0.036	0.275	0.020
0.2:1	0.331	0.011	0.576	0.228	0.217	0.047
2:1	0.390	0.081	0.272	0.050	0.238	0.032
8:1	0.203	0.040	0.183	0.033	0.211	0.006
20:1	0.177	0.042	0.187	0.004	0.187	0.021

At the 7:1 C:P ratio, the DTSSP NPs displayed a positive linear relationship between diameter and X:P ratio, but this relationship does not hold for either of the other C:P ratios. Both the 11:1 and the 17:1 C:P ratios produced 2.5 µm diameter aggregates at low crosslinking densities. The low PDI and similar diameters suggest, however, that the µm-scale aggregates form in a conserved manner. At the 11:1 and 17:1 C:P ratios, there may be more copolymer than necessary to fully encapsulate the protein, and thus charge repulsion or steric hindrance may cause loosely encapsulating PLL-g-PEG strands to branch away from the DTSSP NP. If one DTSSP NHS

group reacts with a branching PLL-g-PEG the length of the effective crosslinker is increased, which may lead to interparticle crosslinking and DTSSP NP aggregation. At higher X:P ratios, the increased concentration of crosslinker and crosslinker-reactive residues may draw loosely associated PLL-g-PEG back to the DTSSP NP surface and reduce DTSSP NP aggregation, which was observed at the 17:1 C:P ratio where increasing X:P ratio corresponded to decreasing DTSSP NP diameter. Regardless, μm-scale particle aggregates are larger than the sub-50 nm diameters desirable for DTSSP NPs to maintain an extended circulation half-life *in vivo* [279].

Protein encapsulation was determined using SDS-PAGE (Figure 5). DTSSP NP samples were loaded onto an 8% SDS-PAGE gel by C:P and X:P ratios. Column 1 displays DTSSP NPs with a 7:1 C:P ratio. As the X:P ratio increased, the band corresponding to free BSA grew fainter before disappearing at the 2:1 X:P ratio. At this X:P ratio, thick smearing was evident at the top of the gel resulting from the increased DTSSP NP size and thus reduced relative migration. At the 8:1 and 20:1 X:P ratios, a faint additional band appeared below the BSA monomer once DTSSP had saturated the lysine residues of the PLL-g-PEG. Column 2 contains DTSSP NPs with an 11:1 C:P ratio. As with the previous gels, increasing X:P showed lightening bands of free BSA until complete encapsulation was achieved with the 2:1 X:P ratio. Once again, the 2:1 X:P ratio produced a thick streak at the top of the gel, and excess DTSSP appeared at the 8:1 and 20:1 X:P ratios. The third column contains DTSSP NPs with a 17:1 C:P ratio, which showed similar trends observed with the 7:1 and 11:1 C:P DTSSP NPs. As expected, the bands of excess DTSSP were less evident at the 8:1 and 20:1 X:P ratios than they were at lower C:P ratios. There was also non-uniform smearing in the 17:1 C:P sample lacking DTSSP, which was likely a gel artifact as it was not observed on other replicates.

The results displayed on the gels were consistent with the mechanism by which the DTSSP NPs were crosslinked. When introduced to PLL-g-PEG encapsulating BSA, the terminal NHS groups of the DTSSP reacted with free amines on the PLL to crosslink the self-assembled polymer

32

network. With no crosslinking, the nanoparticles were held together only through electrostatic interactions and were disrupted by SDS. With the encapsulating structure disrupted, BSA was separated from PLL-g-PEG and observed at the same relative migration as free BSA. As the X:P ratio increased, more DTSSP was available to crosslink free lysine residues, leading to increased structural stability and protein encapsulation. Once the 2:1 X:P ratio was reached, the protein was fully encapsulated and stabilized within the copolymer (Figure 5B), which produced a smearing at the top of the gel due to increased hydrodynamic diameter and size distribution over the free protein.

As the X:P ratio increased to 8:1 and 20:1, the available DTSSP exceeded the available lysine residues, which resulted in the appearance of an excess DTSSP band below the BSA monomer. Additionally, as the number of free lysine residues increased with increasing C:P, the amount of excess DTSSP decreased, as shown by DTSSP band intensity decreasing with increasing C:P for a given X:P ratio. As such, the DTSSP NPs with the 8:1 and 20:1 X:P molar ratios reached crosslinker saturation at the 7:1 and 11:1 C:P ratios. Saturating the PLL-g-PEG is one strategy to ensure complete protein encapsulation and a stable DTSSP NP, but complete crosslinking may lead to difficulty releasing the protein in the targeted environment. The DTSSP NPs synthesized at the 7:1 C:P ratio and the 2:1 X:P ratio were selected for further testing because they displayed complete protein encapsulation, showed a hydrodynamic diameter of 23.5±2.96 nm, and required no purification to remove excess DTSSP. While this DTSSP NP configuration displayed a PDI of 0.39, it could be elevated partly due to its smaller size relative to the other nanoparticles. Consequently, the benefits of smaller size and complete encapsulation were the primary considerations in nanoparticle selection for further characterization.
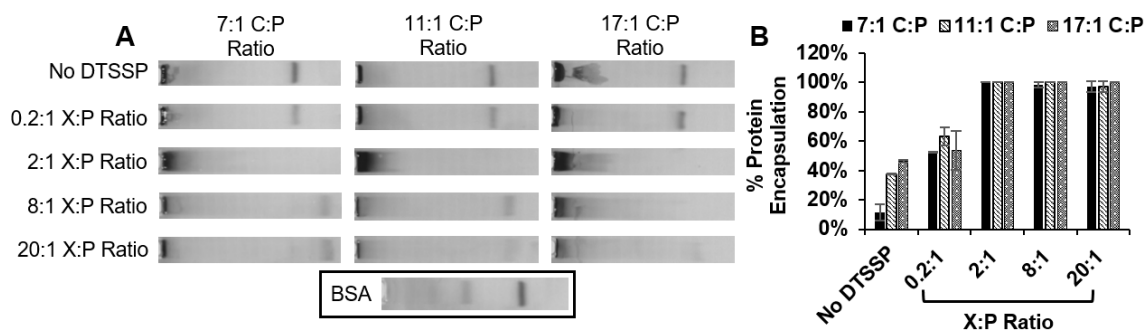
Figure 5: Encapsulation efficiency of nanoparticles synthesized by encapsulating bovine serum albumin (BSA) in poly(L-lysine)-grafted-poly(ethylene glycol) and crosslinked with DTSSP (DTSSP NPs). A library of DTSSP NPs was assembled by varying the copolymer to protein (C:P) and crosslinker to protein (X:P) mass ratios. A) Encapsulation was measured using SDS-PAGE, with a dark band corresponding to free BSA (below) designating unencapsulated protein. B) ImageJ analysis showed complete encapsulation was achieved for each C:P ratio at 2:1 X:P.

3.3.2. DTSSP NP structure and morphology

To determine the effect of DTSSP crosslinking on the surface charge of the nanoparticle, the ζ-potential was measured as an average of 30 converged calculations using phase angle light scattering and found to be 11.9 ± 5.1 mV. As the ζ-potential of BSA alone is -22 mV at pH 6.5 and -32 mV at pH 9, the positive DTSSP NP ζ-potential shows that the remaining cationic amine groups and the hydrophilic PEG on the encapsulating copolymer effectively shielded the charge of the loaded protein [280]. This positive surface charge may be advantageous, as positively-charged nanoparticles display enhanced cellular uptake due to electrostatic interactions with negatively-charged glycosaminoglycans on the cell membrane [281]. Cancer cell membranes are especially anionic due to translocation of inner-layer phosphatidylserine, anionic phospholipids, and proteoglycans, which shows promise for future DTSSP NP cellular uptake studies [281-284].

The structure and size distribution of the DTSSP NPs was confirmed using SEM (Figure 6A). The DTSSP NPs displayed consistent elliptical morphology with few variations. ImageJ analysis of 151 particles revealed a range of diameters from 11 to 55 nm with a median particle equivalent diameter of 16.3 nm (Figure 6B). Based on the size distribution, the concentration of the DTSSP NPs was estimated as 1.6 µM with an average loading of 1.7 BSA per DTSSP NP. TEM was used to determine the internal structure and morphology of the DTSSP NP (Figure 6C). The dark rings correspond to reduced electron transmission whereas the centers display increased electron transmission, which is consistent with a core-shell morphology of a low-density center surrounded by a high-density coating. DTSSP NP sizes ranged from 14 to 100 nm, and the elliptical morphology was consistent with that observed with SEM.
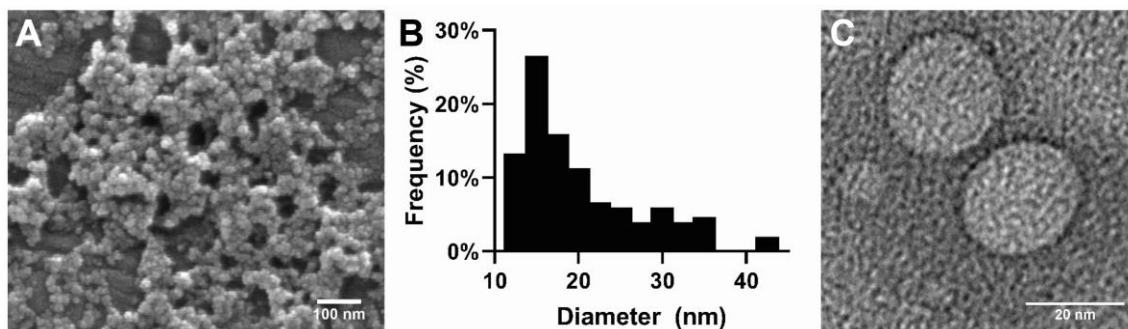
Figure 6: Electron microscopy of nanoparticles crosslinked with DTSSP. The scanning electron micrograph (A) was analyzed using ImageJ to determine the size distribution (B) from 151 nanoparticles, and a median diameter of 16.3 nm was observed. The transmission electron micrograph (C) shows core-shell morphology, with a high transmission center encompassed by a low transmission halo.

3.3.3. Retention of esterolytic activity

Therapeutic protein delivery necessitates that the protein must retain medicinally relevant properties throughout the encapsulation and release processes. A prior study with

butyrylcholinesterase suggested that PLL-g-PEG/protein complexes crosslinked with glutaraldehyde retained the activity of the encapsulated enzyme [285]. DTSSP NP maintenance of encapsulated protein function was measured spectrophotometrically using the esterolytic breakdown of NPA to 4-nitrophenol. Though previously disputed, BSA displays moderate esterolytic activity based around active site Tyr411 [274]. Enzymatic binding and cleaving of the substrate was not hindered by encapsulation, which suggests that encapsulation did not detrimentally affect protein function. Both the Non-X NPs and the DTSSP NPs displayed higher product concentrations than free BSA at all time points (Figure 7). The enzymatic activity was enhanced by the addition of the copolymer both with and without crosslinking. The PLL-g-PEG showed pseudoesterolytic activity that was reduced when crosslinked with DTSSP, whereas DTSSP crosslinking enhanced the esterolytic activity of BSA encapsulated within PLL-g-PEG. This observation is corroborated by previous studies and has been attributed to an increased local substrate concentration within the nanoparticle leading to an increase in reaction rate [26, 286].
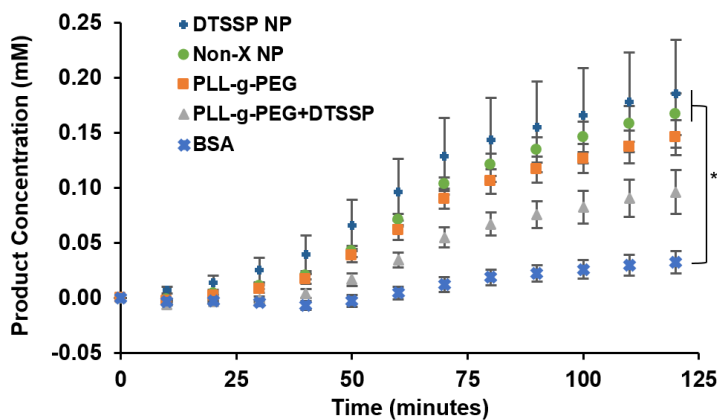
Figure 7: Esterolytic activity of nanoparticles made from bovine serum albumin (BSA) encapsulated in poly(L-lysine)-grafted-poly(ethylene glycol) and crosslinked with DTSSP (DTSSP NP). Samples were incubated with 2.4 mM 4-nitrophenyl acetate and absorbance at 410

nm was used to determine the product concentration. Both the non-crosslinked nanoparticle

(Non-X NP) and the DTSSP NP showed significantly higher product concentrations than the free

protein due to an increase in the local substrate concentration within the nanoparticle. The PLL-g-

PEG showed pseudoesterolytic activity that was reduced when crosslinked with DTSSP, whereas

DTSSP crosslinking enhanced the esterolytic activity of BSA encapsulated within PLL-g-PEG. *

designates p-value < 0.05.

3.3.4. DTSSP NP stability

3.3.4.1. Stability in heparin

Heparin sulfate and numerous serum proteins display a net negative charge that could interfere

with the electrostatically self-assembled nanoparticles. As such, the level of DTSSP NP

susceptibility to polyanions was determined through a fluorescence assay. The results of DTSSP

NPs co-incubated with 0.27 mM heparin are displayed in Figure 8A. There was no difference

between the fluorescence of the DTSSP NPs incubated with heparin and those without heparin,

which suggests that polyanions had a negligible effect on the stability of the crosslinked

nanoparticles.

3.3.4.2. Stability in serum

The DTSSP crosslinked PLL-g-PEG coating is designed to encapsulate a protein delivered

intravenously. Consequently, protein retention in the presence of serum is essential, as serum

stability directly impacts the circulation half-life *in vivo* [287]. The fluorescence assay for serum

stability showed that the presence of FBS has a minor effect on the protection and encapsulation

of proteins within DTSSP NPs (Figure 8A). After 22 hours of incubation, 5% and 10% FBS

displayed a 10% and 11% increase in fluorescence with SDS denaturation respectively, but 25%

FBS only showed a 3% increase over the fluorescence exhibited by the DTSSP NPs in PBS.

Though incubation in serum displayed minor protein release, the DTSSP NPs resisted extensive destabilization in the presence of serum proteins.

3.3.4.3. Protection against proteases

The ability of the DTSSP NPs to protect an encapsulated protein from degradation by proteases was confirmed using fluorescence spectroscopy. When incubated with 0.1 mg/mL chymotrypsin, the DTSSP NPs displayed reduced protein degradation in comparison to free DQBSA for up to 42 hours (Figure 8B). The percentage of degraded free DQBSA increased quickly at the start of the reaction, requiring 1.3 hours to reach 50% degradation after introduction of the protease, whereas 50% degradation was reached for the DTSSP NPs 10 hours after protease introduction. The degradation of DTSSP NPs displayed a more gradual upward trend in comparison to the sharp upward curve of DQBSA and the Non-X NPs, suggesting that crosslinking with DTSSP reduced the exposure of the encapsulated protein to other proteins in the immediate environment. This resulted significant protein protection at 12 hours (p-value < 0.001), 24 hours (p-value < 0.005), and 36 hours (p-value < 0.05).

Though DTSSP NPs showed enhanced protective properties over DQBSA and Non-X NPs in the presence of chymotrypsin, the degradation trend upward mirroring the aforementioned samples suggests that protection was not permanently conveyed to the encapsulated protein. In contrast, the non-cleavable DSS-crosslinked nanoparticles displayed only minor degradation before reaching a plateau. As such, a small amount of superficial protein experienced degradation initially, but most protein was retained and protected within the non-reducible DSS crosslinked structure.

Since the DSS NPs displayed the same molar crosslinking density and spacer arm length as the DTSSP NPs, other factors must explain the difference observed in protease protection. As DSS lacks water solubility, it was dissolved in DMSO before being used to crosslink the DSS NP. This

variation in solvent may have led to a reduction in surface adjacent DQBSA and thus reduced fluorescence in the presence of chymotrypsin. While this may account for part of the observed difference, further explanation is warranted to better explain the observed difference in protein degradation.

As the primary difference between the DSS NPs and DTSSP NPs is the inclusion of a disulfide, this bond likely played a role in the variation of protection against proteases. The χ_3 torsional angle, which is the rotation of the β-carbon atoms around the disulfide, is critical to disulfide stability [288-290]. If these angles are not maintained, the strain within the bond may increase drastically [291]. As the disulfide in DTSSP is not maintaining the conformation of a single protein but is rather maintaining stability of a self-assembled copolymer encapsulating a protein, many disulfides could be under enhanced strain. This enhanced strain may result in a DTSSP NP with lower stability than the DSS NP as observed when each was incubated with chymotrypsin.
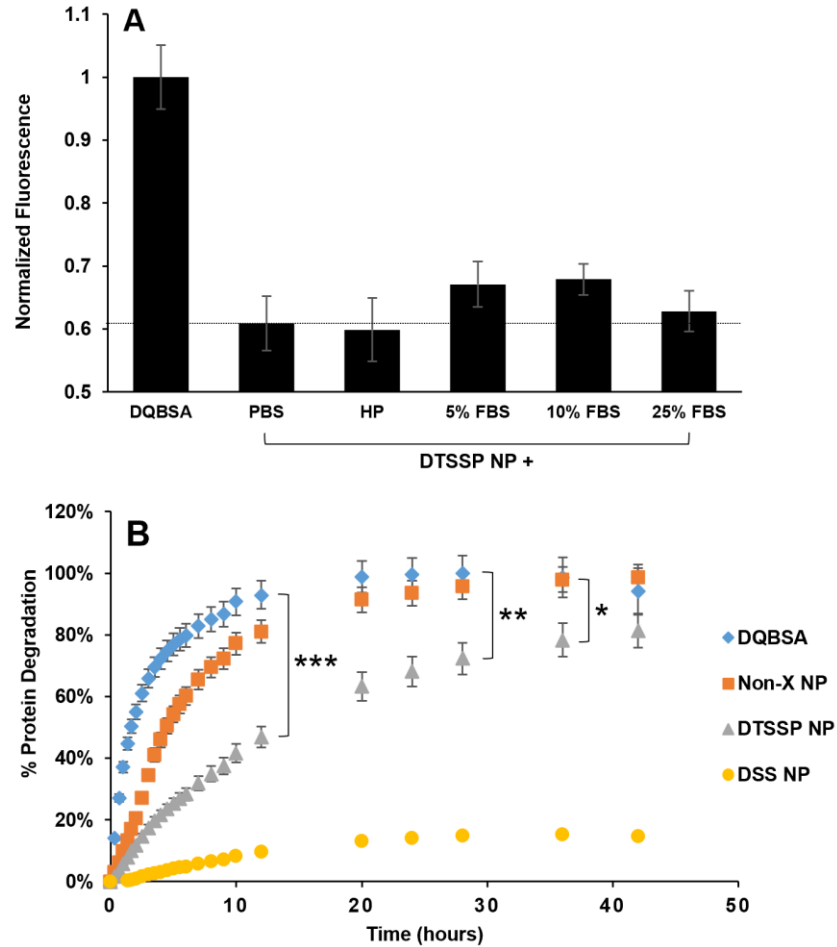
Figure 8: Stability results for nanoparticles of DQ Green BSA encapsulated in poly(L-lysine)-grafted-poly(ethylene glycol). A) Fluorescence greater than the dotted line designates protein released from the DTSSP NP. No protein release was observed from DTSSP NPs incubated with 0.27 mM heparin, and insignificant protein release was observed when incubated with varying concentrations of fetal bovine serum (FBS). B) Protein degradation in the presence of 0.1 mg/mL chymotrypsin. The free protein (DQBSA) and non-crosslinked nanoparticle (Non-X NP) showed rapid protein degradation, while the non-cleavable crosslinker DSS provided strong protection for the encapsulated protein (DSS NP). The DTSSP NP effectively protected the encapsulated protein for over 24 hours. * designates a p-value < 0.05, ** designates p-value < 0.005, and *** designates p-value < 0.001.

3.3.5. Nanoparticle destabilization in a reductive environment

While strong protective properties are desired in the presence of serum and proteases, nanoparticle destabilization in a reductive environment is foundational to the successful delivery of tumor-targeted therapeutic proteins using crosslinked PLL-g-PEG. DTSSP NP destabilization was measured based on the fluorescence of DQBSA when denatured with SDS (Figure 9). DTT was selected as a reducing agent because its unimolecular reduction mechanism was uninhibited by SDS [292]. Before the addition of DTT, the fluorescence of the DTSSP NPs was half of that observed with DQBSA alone, while DSS NPs displayed 40% of the normalized DQBSA fluorescence. From previous SDS-PAGE findings, the protein was fully encapsulated within both the DTSSP NPs and the DSS NPs, and the difference in initial fluorescence was likely due to enhanced quenching induced by the permanent crosslinker. Based on these observations, the fluorescence of free DQBSA in DTT was utilized as the baseline for 100% protein release, while the fluorescence of the DTSSP NP in PBS was used as the baseline corresponding to 100% encapsulation. DQBSA, DTSSP NPs and DSS NPs were incubated with 0.20 mM, 1.0 mM, and 5.0 mM DTT at 37°C, and protein release was measured as a function of time.

When incubated with PBS only, the DTSSP NPs and DSS NPs both displayed fluorescence significantly lower than that of DQBSA. With the addition of DTT and twelve hours of incubation, however, the relative fluorescence of the DTSSP NPs increased while that of the DSS NPs remained low (Figure 9A). Furthermore, the fluorescence of DTSSP NPs increased with increasing DTT concentrations, showing that the rate of protein release was affected by the concentration of reducing agents in the surrounding environment. When converted to a ratio of protein released, twelve hours of incubation in 0.20 mM, 1.0 mM, and 5.0 mM DTT corresponded to protein release of 56% $\pm$ 7%, 79% $\pm$ 9%, and 81% $\pm$ 9%, respectively.

The protein release profile was plotted as a function of time (Figure 9B). With 5 mM DTT, over 50% of the total protein was released within the first two hours, and after six hours over 75% of the protein had been released. Subsequently, the protein release rate decreased and achieved a maximum of 81% after 12 hours incubation. Lower concentrations of DTT displayed reduced rates of protein release. At 1.0 mM DTT, 50% protein release was achieved after 5 hours of incubation, and over 75% was achieved after 12 hours. This 1.0 mM DTT release profile must be considered the upper bound for protein release that could be observed *in vivo* due to the lower reduction potential of GSH in comparison to DTT [293, 294]. The lowest concentration of DTT tested, 0.20 mM, showed a further reduction in protein release profile, with only 56% protein release achieved after 12 hours. As the reduced DTT concentration corresponded to increased DTSSP NP stability, this delivery strategy shows potential to selectively destabilize the copolymer coating in an upregulated redox environment while maintaining encapsulation and protective properties in non-reducing environments.

Several factors may play a role in the incomplete protein release. Reduced DTSSP has been shown to undergo thiol exchange and subsequent disulfide scrambling, so it could be that reduced DTSSP inhibited measurement of protein release through aggregate formation [295, 296]. Furthermore, BSA has been shown to form aggregates in a reductive environment, which can cause fluorescence quenching and lower the fluorescent signal of free protein [297]. Though incubation with SDS should have reduced the aggregation effect, some quenching may have been responsible for the fluorescence of the DTSSP NP in DTT being less than that of DQBSA after twelve hours of incubation. This should not affect *in vitro* or *in vivo* studies however, as disulfide scrambling decreases in acidic pH [295, 296, 298]. Thus, disulfide scrambling and aggregate formation may explain the minor retention of fluorescence quenching in the presence of DTT.
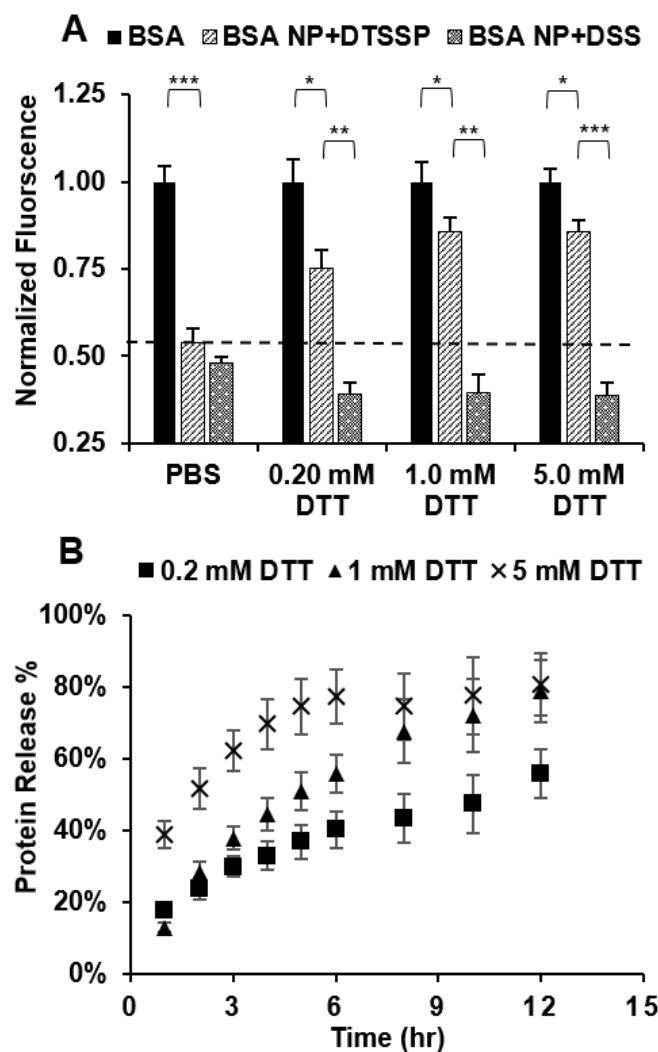
Figure 9: Nanoparticle destabilization in a reductive environment and protein release from nanoparticles encapsulating DQ Green BSA (DQBSA) within poly(L-lysine)-grafted-poly(ethylene glycol) and crosslinked with disulfide-containing DTSSP (DTSSP NPs). A) Normalized fluorescence of DQBSA, DTSSP NPs, and DQBSA nanoparticles crosslinked with DSS (DSS NP), a non-reducible DTSSP analog, after twelve hours incubation with phosphate buffer saline (PBS) and 0.20, 1.0, and 5.0 mM DTT. The dotted line corresponds to complete encapsulation within the DTSSP NP. * designates p-value < 0.05, ** designates p-value < 0.005, and *** designates p-value < 0.001. B) Protein release profile for DTSSP NPs in the presence of DTT.

3.4. Conclusions

DTSSP was an effective crosslinker for incorporating redox-responsive properties into poly(L-lysine)-grafted-poly(ethylene glycol) (PLL-g-PEG) polymer-protein nanoparticles (DTSSP NPs). A library of DTSSP NPs was made by varying the copolymer to protein (C:P) and crosslinker to protein (X:P) mass ratios. Dynamic light scattering and gel migration assays showed that therapeutically-relevant nanoparticles can be synthesized using an 11% PEG grafting ratio, a C:P ratio of 7:1, and a X:P ratio of 2:1. The stabilized nanoparticles fully encapsulated the available protein, retained the protein's enzymatic activity, protected the encapsulated protein from protease degradation, and displayed stability in solutions containing heparin and serum. Furthermore, the DTSSP NPs were effectively destabilized in the presence of dithiothreitol, which suggests that PLL-g-PEG crosslinked with DTSSP may be effective for selectively delivering anti-cancer proteins to the localized environment of a tumor. This work contributes to understanding the medical applications of self-assembled cationic polymer-protein nanoparticles through incorporation of environmentally responsive moieties. Further research in this area should continue to contribute to our understanding of delivering therapeutic proteins to medicinally relevant areas of the body.

CHAPTER IV

A RAPID MILLIFLUIDIC SYNTHESIS OF TUNABLE POLYMER-PROTEIN

NANOPARTICLES

4.1. Introduction

Protein delivery is central to the treatment of numerous maladies, and nanoparticle drug delivery

shows potential to enhance the well-established efficacy of current therapeutics [31].

Nevertheless, hurdles to protein delivery include rapid *in vivo* clearance, side effects, aggregation,

denaturation, degradation, weak delivery to intracellular locations, and immunogenicity [3, 4].

Nanoparticle formation may overcome these hurdles by encapsulating therapeutic proteins in a

functional and biocompatible shell [4]. Polymers are among the best materials for drug delivery

due to their low toxicity [4, 299] and ability to control protein delivery [9, 11, 12]. Furthermore,

polymer-encapsulated proteins can be used for both intracellular and extracellular therapies, and

nanoparticle functionality can be tuned with respect to the biological properties of a targeted

environment [9].

The materials utilized in polymer-protein nanoparticles determine the mechanism by which

encapsulation occurs. Cationic polymers can self-assemble around proteins through electrostatic

interactions [26, 300]. Poly(L-lysine) has been utilized in this application due to its charge and

the versatility of the primary amine functional group, which facilitates simple crosslinking and

chemical modification [136, 301]. Cationic polymer nanoparticles are recognized as foreign

bodies *in vivo* [302], however, so hydrophilic materials such as poly(ethylene glycol) (PEG) are commonly utilized to reduce nonspecific protein adsorption and elimination by the innate immune system [13-15]. PEG can be conjugated to lysine residues to confer a hydration layer and enhance the biocompatible characteristics of the copolymer [303]. As such, a copolymer composed of both PLL and PEG can self-assemble around proteins while reducing their immunogenicity, aggregation tendency, and clearance rate [136, 304, 305].

Most self-assembled polymer-protein nanoparticles are synthesized in batch processes. While bulk mixing is a simple and practical strategy for nanoparticle development, its discontinuous nature offers few factors for tuning and presents challenges in controlling particle size and distribution [23, 219]. Continuous flow systems show potential to overcome these limitations [219]. Microfluidics have been proposed as an alternative to bulk mixing for the preparation of monodisperse nanoparticles. The µm-scale channels utilized in microfluidic systems reduce diffusional lengths, resulting in enhanced mass transfer and a homogeneous environment that allows control over the properties of the nanoparticles [220-222]. Furthermore, variations in microfluidic system configuration have been shown to affect mass transfer and consequently the size and dispersity of synthesized nanoparticles [306]. Additional benefits of microfluidics include reproducibility, simplicity, versatility, and enhanced safety [222-224].

Similarly, millifluidic configurations share the advantages of microfluidics while simultaneously boasting reduced cost and improved process controls [219, 225]. Furthermore, millifluidics are more resistant to fouling than microfluidics and more easily maintain an isothermal and homogeneous chemical environment [220, 226]. Until now, microfluidics have been primarily used in the synthesis of inorganic nanostructures, whereas the millifluidic synthesis of organic nanoparticles has been limited [227, 228]. When utilized for therapeutic nanoparticle synthesis, millifluidic processes have proven successful at matching the characteristics of nanoparticles produced in batch processes [225] and have shown better size control than comparable batch

processes [23]. One study directly compared a millifluidic process to a bulk mixing process in synthesis of drug-loaded nanoparticles and found that the millifluidic process displayed enhanced drug loading over the batch process [220]. As such, millifluidics have been shown useful for small molecule drug delivery system applications and show benefits over similar batch processes.

Ultrasonication has been widely used within millifluidics for its ability to enhance transport properties and reduce activation energy [231-237, 307]. Furthermore, ultrasound has been shown to reduce fouling and induce uniform mixing in flow processes through incitation of cavitation [237, 238]. Acoustic frequencies between 20 kHz and 1 MHz create bubbles matching the scale of millifluidic channels, which can magnify the mixing effect through resonance [237, 239, 240]. With such prior evidence, application of ultrasound to millifluidic polymer-protein nanoparticle synthesis displays potential for controlled mixing in the laminar flow regime.

In this work, bovine serum albumin (BSA) was encapsulated in poly(L-lysine)-grafted-poly(ethylene glycol) using a millifluidic synthesis process that incorporated ultrasound to introduce controlled mixing in a laminar flow regime. The objective of this research was to present a rapid continuous process capable of producing stable, tunable polymer-protein nanoparticles. Nanoparticle diameters were measured as a function of feed flow rate and system configuration and were characterized by morphology, polydispersity index, encapsulation efficiency, ζ-potential, stability, and retention of enzymatic activity.

4.2. Materials and methods

Lyophilized bovine serum albumin (BSA), 4-nitrophenyl octanoate, and poly(L-lysine)-HBr (PLL-HBr) of 15-30 kDa molecular weight were purchased from Sigma Aldrich (St. Louis, MO). Poly(ethylene glycol) of 5 kDa molecular weight functionalized with a carboxymethyl succinimidyl ester (mPEG-NHS) was purchased from Creative PEGworks (Durham, NC). Glutaraldehyde (GA, 50%), acrylamide/bisacrylamide (37.5:1) and other polyacrylamide gel

47

casting and running materials were purchased from Fisher Scientific (Pittsburgh, PA). DQ Green BSA was purchased from Life Technologies (Grand Island, NY). Millifluidic tubing and junctions were purchased from McMaster-Carr (Elmhurst, IL). Phosphate buffer saline (PBS, 10 mM) was made in-house.

4.2.1. PLL-g-PEG copolymer synthesis

Poly(ethylene glycol) was grafted to poly(L-lysine) according to the methods described by Flynn et al. [26], in which succinimidyl ester functional groups on mPEG-NHS were reacted with primary amines on PLL to create a grafted copolymer. A solution containing 15 mg of PLL-HBr in 200 μL PBS was made before 57 mg of 5 kDa mPEG-NHS was added to match the desired 10% PEG grafting ratio. The copolymer (PLL-g-PEG) solution was incubated at 25°C for 2 hours before washing with 300 μL ultrapure water three times using a Pierce™ Protein Concentrator with a 10 kDa molecular weight cutoff (MWCO, ThermoFisher Scientific, Waltham, MA). After washing, four samples were combined, diluted to 1 mL in ultrapure water, and stored at -80°C overnight. The following day, the frozen copolymer solution was removed from the freezer and freeze dried for 24 hours. The achieved grafting ratio of PEG to PLL was calculated from the ^{1}H NMR spectrum. Lyophilized copolymers were stored at -20°C until use.

4.2.2. Preparation of feed solutions

Protein and copolymer feed solutions were prepared immediately prior to use. The BSA solution was made by adding 20 mg lyophilized BSA to 10 mL PBS and allowing it to dissolve for 30 minutes. The solution was then filtered through a pre-wetted 0.20 µm syringe filter to remove large aggregates before the absorbance at 280 nm was measured and used to determine the protein concentration. The BSA solution was subsequently diluted to 0.266 mg/mL in PBS and stored at room temperature. The copolymer feed solution was prepared by removing lyophilized PLL-g-PEG from the freezer, warming it to 25°C, and dissolving it in PBS to 1.8 mg/mL.

4.2.3. Millifluidic nanoparticle synthesis

The millifluidic system was constructed from 1/16-inch inner diameter (ID) tubing. The tubing material used in this work was clear fluorinated ethylene propylene (FEP) for system Configurations A, B, and C, and silicone rubber for Configurations D and E (Table 2). In Configurations A, B, and C, 100 cm of FEP tubing was cut and connected to two separate 10 cm lengths of silicone rubber tubing with a 3-way barbed tee junction. Similarly, in Configurations D and E, 100 cm of silicone rubber tubing was cut and connected to two 10-cm lengths of silicone rubber tubing.

Syringe-to-tubing adapters were modified from 200 µL micropipette tips that had each been transected one cm from the tip and 0.5 cm from the base. The narrow ends of the transected micropipette tips were inserted into the open ends of the silicone rubber tubing extending from the tee junction. All connections were externally sealed with super glue that was allowed to cure for 4 hours. Before initial use, the sealed tubing was disinfected with 70% ethanol, rinsed with ultrapure water, and dried with forced air. The tubing was fastened to an ultrasonic water bath with clear adhesive such that there was a 10 cm length of tubing between the tee junction and the water surface and a 15 cm length of tubing from the water surface to the tube outlet (Configurations A, B, C, and D). The tubing within the ultrasonic bath was coiled (8 cm diameter) to ensure the tubing did not contact the base or walls of the bath. A Fusion 200 syringe pump (Chemyx Inc., Stafford, TX) was placed adjacent to the sonic bath to run both the PLL-g-PEG and BSA feed solutions. The 5 mL feed syringes used to inject the solutions into the system syringes (Becton Dickinson and Company, Franklin Lakes, NJ) were filled with BSA (0.266 mg/mL) and PLL-g-PEG (1.8 mg/mL) solutions. The loaded syringes were then placed on the rack of the syringe pump.

Configuration E was a development on Configuration D. In Configuration E, the silicone tubing was extended an additional 100 cm using a secondary tee junction connecting the outlet of the first 100 cm of tubing to the inlet of the second 100 cm, which allows for future in-line addition of crosslinking reagents. A 5-cm length of silicone rubber tubing was connected to the secondary tee junction, and this additional input port was filled to the junction with a PBS-loaded 5 mL syringe to prevent reagent diversion. Ninety of the initial 100 cm of tubing were submerged in the ultrasonic bath, whereas the final 100 cm was elevated from the ultrasonic bath to form the post-sonication laminar flow quiescent zone.

All nanoparticle synthesis operations were performed at room temperature. Preparation was completed by setting the syringe pump flow rate, securing a microcentrifuge tube at the terminus of the millifluidic tubing, and activating the ultrasonic bath. The syringe pump was operated until the entire volume of the feed solutions had been fed to the system to form electrostatically self-assembled millifluidic nanoparticles (MFNPs) (Figure 10). Upon completion, 500 μL of MFNPs were placed in a microcuvette and loaded into a ZetaPALS ζ-potential analyzer (Brookhaven Instruments Corporation, Holtsville, NY). The hydrodynamic diameter and polydispersity index (PDI) of the nanoparticles were calculated from 5 dynamic light scattering (DLS) measurements taken at a 90° angle for 30 seconds each. Following DLS, the samples were transferred to a 2 mL microcentrifuge tube and crosslinked under gentle vortexing with 76.8 μL of 0.025 wt% glutaraldehyde. The crosslinked MFNPs were incubated at room temperature for 3 hours before being stored at 4°C until further use. The millifluidic system was rinsed twice with deionized water and dried with forced air between experiments. Table 2 displays the mean velocity, residence time, and Reynolds number at study-relevant flow rates.
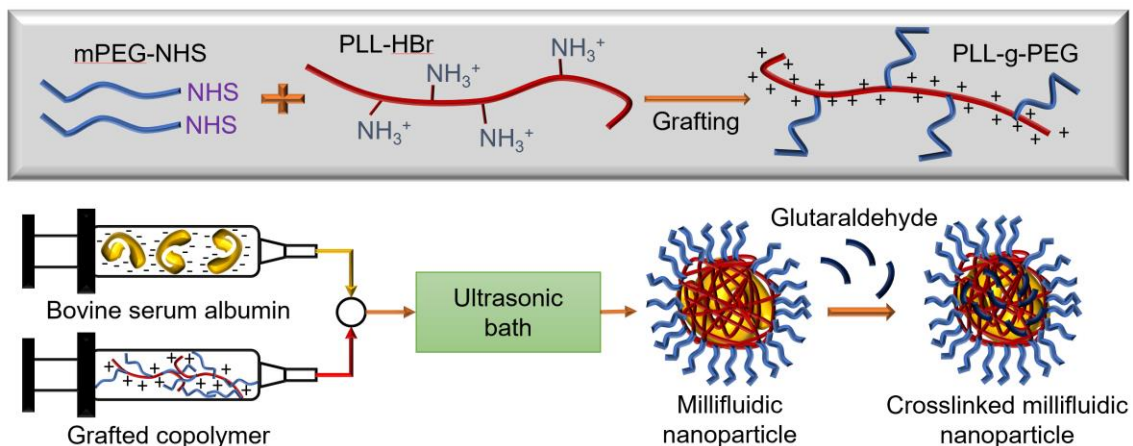
Figure 10: Schematic of the millifluidic synthesis process for encapsulation of bovine serum albumin within poly(L-lysine)-grafted-poly(ethylene glycol). mPEG-NHS of 5 kDa molecular weight was grafted to 11% of the free amines on 15-30 kDa PLL-HBr to create PLL-g-PEG. Nanoparticle formation was accomplished using ultrasonic cavitation to induce electrostatic self-assembly within a millifluidic laminar flow regime. The nanoparticles were stabilized upon exit from the millifluidic system through crosslinking with glutaraldehyde under gentle vortexing.

Table 2: Velocity, residence time, and Reynolds number for flow rates relevant to the millifluidic nanoparticle synthesis

Feed Flow Rate (μL/min)	Mean velocity (mm/s)	Residence time, 75 cm sonication length (min)	Reynold's Number
50	0.84	14.8	1.29
100	1.68	7.4	2.57
150	2.53	4.9	3.86
200	3.37	3.7	5.14
250	4.21	3.0	6.43
300	5.05	2.5	7.72
400	6.74	1.9	10.3

4.2.4. Variation of sonication power

Three ultrasonic baths were used to determine the effect of ultrasound power input on the hydrodynamic diameter of the MFNPs. A Branson 2510MT Ultrasonic Bath (St. Louis, MO) delivered an input power of 100W, whereas the Fisherbrand™ CPXH Series Heated Ultrasonic Cleaning Bath (Fisher Scientific, Pittsburgh, PA) delivered 110W and the VWR B3500A-MT (West Chester, PA) provided 135W. Each of the sonic baths operated at 42±3 kHz and possessed similar geometries.

4.2.5. Nanoparticle ζ-potential measurement

The ζ-potential of glutaraldehyde-crosslinked MFNPs synthesized with Configuration E at 50 and 300 μL/min was measured using a ZetaPALS ζ-potential analyzer. Nanoparticle samples were combined to 1.5 mL in a disposable cuvette, and the ζ-potential was measured using phase analysis light scattering and Smoluchowski's equation. Fifty converged calculations were averaged and reported with standard error as the ζ-potential of the MFNPs.

4.2.6. Scanning electron microscopy analysis

The MFNP size distribution was analyzed using an FEI Quanta 600 scanning electron microscope (ThermoFisher Scientific, Waltham, MA). MFNPs produced with Configuration E at a feed flow rate of 50 μL/min were crosslinked with glutaraldehyde. The MFNP solution (20 μL) was deposited onto an aluminum SEM stub with a drop-casting method and allowed to dry at room temperature for 20 hours. The dried particles were subsequently sputter-coated with gold-palladium on a Cressington 108 sputter coater (Cressington Scientific Instruments, Watford, England). Images were recorded at an accelerating voltage of 20.0 kV, and MFNP size distribution was determined from 436 particles using ImageJ analysis. The size distribution was

used to estimate the concentration and loading of the DTSSP NPs assuming smooth sphere geometry, a 7:1 C:P volume ratio, and a BSA geometry of 4 nm by 4 nm by 14 nm [273].

4.2.7. Transmission electron microscopy analysis

Transmission electron microscopy was used to determine MFNP morphology. MFNPs were synthesized with Configuration E at a feed flow rate of 50 μL/min and crosslinked with glutaraldehyde. A formvar TEM grid was loaded with 10 μL of MFNPs that had been diluted 10:1 in DI water, and the MFNP sample was dried at room temperature for 15 minutes before excess solvent was wicked away. The sample was not stained with a contrast agent before observation using a JEOL JEM-2100 electron microscope (JEOL Ltd., Akishima, Tokyo, Japan) with an accelerating voltage of 200 kV.

4.2.8. Protein encapsulation in millifluidic nanoparticle synthesis

The extent of protein encapsulation within crosslinked MFNPs was measured using a gel migration assay. Samples of crosslinked MFNPs were diluted with non-reducing SDS-PAGE sample buffer at a 1:1 volume ratio. Samples were not boiled but were incubated at 37°C and shaken on a Thermofisher Max400Q orbital shaker (Thermofisher, Waltham, MA) at 80 rpm for 15 minutes before 27 μL aliquots were loaded onto an 8% SDS-PAGE gel. SDS-PAGE gels were run at 200V on a Bio-Rad Tetracell mini gel electrophoresis apparatus (Bio-Rad Laboratories, Hercules, CA) until the dye front reached the bottom of the gel (approximately 45 minutes). The running buffer did not contain SDS. SDS-PAGE gels were stained with Coomassie G-250 before imaging. Relative band intensity was used to determine the extent of protein encapsulation within the MFNPs.

4.2.9. Particle stability against proteases

Stability in the presence of proteases was determined using a fluorescence assay. MFNPs were formed with Configuration E at a flow rate of 50 µL/min using DQ Green BSA (DQBSA) as the encapsulated protein. DQBSA is BSA haptenated with 4,4-difluoro-5,7-dimethyl-4-bora-3a,4a-diaza-s-indacene-3-propionic acid fluorophore (BODIPY FL) to such an extent that it experiences self-quenching relievable through protein denaturation [276]. When incubated with chymotrypsin, free DQBSA displayed a sharp increase in fluorescence, whereas DQBSA protected within the MFNP retained its initial fluorescence. MFNPs were diluted 6.1:1 by volume in PBS and 100 µL aliquots were loaded onto a 96 well plate. α-Chymotrypsin from bovine pancreas was dissolve in PBS to 0.6 mg/mL, and 20 µL of protease solution were added to each well for a final concentration of 0.1 mg/mL. The fluorescence was measured (485 nm excitation, 535 nm emission) using a Beckman Coulter DTX 880 Multimode Detector (Beckman Coulter Life Sciences, Brea, CA) initially and periodically afterwards to determine the MFNP susceptibility to protease degradation.

4.2.10. Retention of enzymatic activity

To determine the effect of encapsulation on protein activity, MFNPs synthesized with Configuration E at 50 and 300 µL/min were incubated with 10 mM 4-nitrophenyl octanoate. Cleavage of 4-nitrophenyl octanoate by BSA produces 4-nitrophenol, which displays an absorption peak at 410 nm and allows the reaction to be monitored spectrophotometrically. MFNPs were removed from storage and diluted 5.9:1 by volume in PBS. Three 100 µL aliquots were added to a Falcon 96 well plate (Corning Inc., Corning, NY), and 20 µL of 60 mM 4-nitrophenyl octanoate in isopropanol was added to each well. The plate was incubated at 37°C, and absorbance at 410 nm was measured periodically using a Packard Spectracount plate reader (Cole-Palmer, Vernon Hills, IL).

4.2.11. Statistical analysis

Statistical analysis was performed in Microsoft excel using a two-tailed heteroscedastic student's t-test. A minimum of 3 samples were used for each measurement. Single measurements displaying values greater than 1.5 times the interquartile range away from the nearest quartile (Q1 or Q3) were classified as outliers and ignored when calculating average nanoparticle diameter.

4.3. Results and discussion

4.3.1. Nanoparticle size variation with volumetric flow rate

The achieved grafting of PEG to PLL was calculated as 11% from ^{1}H NMR spectra Preliminary trials without ultrasonication produced µm-scale polymer-protein aggregates. Each of the first three system configurations tested with ultrasonication (A, B, and C from Table 2) produced MFNPs between 150 and 300 nm in diameter and exhibited a minimum diameter corresponding to a feed flow rate between 100 and 300 µL/min (Figure 11A). With Configuration A, DLS measurements showed a MFNP diameter of 153 nm at 150 µL/min. The diameter increased to 256 nm and 239nm at 40 µL/min and 350 µL/min, respectively. This suggests that there was an optimal range of acoustic energy input to induce mixing that forms nm-scale complexes of PLL-g-PEG and BSA.

To test this hypothesis, the 100W sonication bath from Configuration A was replaced with an 110W model (Configuration B). With the higher power input, DLS analysis showed a MFNP diameter of 164 nm at a flow rate of 200 µL/min. The observed MFNP diameter again increased at higher and lower feed flow rates, reaching 194 nm at 100 µL/min and 205 nm at 400 µL/min. This trend supported the hypothesis of a favorable range of ultrasonic energy input for MFNP formation. Subsequently, Configuration C replaced the ultrasonic bath with a 135W model, and a trend similar to that of the two previous system configurations was observed. With Configuration

C, the MFNP diameter at 250 μL/min was measured as 149 nm, with MFNP diameters of 192 nm

and 182 nm measured at flow rates of 50 and 400 μL/min, respectively.

Variation in power input to the system had minimal effect on the diameter of the MFNP

produced, but it did affect the flow rate at which the minimum particle diameters were observed.

The flow rate producing the smallest observed nanoparticle size was lowest with Configuration

A, which also displayed higher MFNP diameters at the maximum and minimum flow rates than

either Configuration B or C. In contrast, the flow rate producing the smallest MFNP diameter was

highest for Configuration C while the diameters at the maximum and minimum flow rates were

smaller than those of Configuration A or B. These data seem to suggest an upward-opening

parabolic relationship between feed flow rate and MFNP diameter that widened and shifted right

with increasing ultrasonic power input.

Along with hydrodynamic diameter, the polydispersity index (PDI) of the MFNPs was measured

for each of these system configurations (Figure 11B). PDI generally varied between 0.2 and 0.3

and increased with increasing flow rate. Configuration A generally displayed the lowest PDI,

with the lowest flow rates displaying highly uniform particles and PDI approaching 0.1. This

observation suggests that lower power input corresponded to enhanced mixing consistency and

more homogenous MFNPs and increased flow rates correspond to decreased mixing consistency.

Consequently, while a single MFNP diameter could be produced at two different flow rates, the

PDI was generally lower at the lower flow rate.

4.3.2. Nanoparticle size variation with tubing material

The effect that the tubing material had on MFNP diameter was determined by replacing the FEP

tubing utilized in the previous configurations with silicone rubber tubing (Configurations D and

E). When the system was operated at 50 μL/min, the particle size decreased dramatically from the

previous value of 192 nm to 26 nm (Figure 11A, Configuration C compared to D). This result is

particularly desirable because it shows that the millifluidic system can produce nanoparticles of size similar to and smaller than those made with the batch process [26]. Interestingly, the MFNP diameter remained low with increasing flow rate without displaying a trend toward increasing size. The remarkable decrease in particle size with the change in tubing material suggests that the flexible silicone rubber improved the mixing characteristics within the millifluidic channel in comparison to the more rigid FEP tubing. Energy transmission through the millifluidic tubing appears to be essential for controlling the mixing that occurs in the millifluidic channel, and that improved mixing can rapidly synthesize MFNPs smaller than 30 nm.

These small MFNP sizes are of particular interest for controlled administration of therapeutics. As the hydrodynamic diameter of BSA alone is approximately 8 nm, a MFNP diameter below 15 nm suggests individual loading of proteins within a PLL-g-PEG shell. This precise control over protein loading is especially advantageous when considering extrapolation to encapsulation of therapeutic proteins that may differ from BSA in size, morphology, and surface charge. The consistency of MFNP sizes with varying flow rates could be due to the flexible silicone rubber providing enhanced transmission of sonic waves between the system and the surroundings in contrast to the more rigid FEP tubing. Ultrasonic energy transmission is based on losses through the medium and at the solid-liquid interfaces, and thus the attenuation of the ultrasonic impulse was reduced in the flexible silicone rubber tubing in comparison to the FEP tubing [308]. This enhanced transmission resulted in improved mixing and smaller MFNP sizes.

Despite the favorable results in MFNP diameter, the PDI from the silicone rubber tubing ranged between 0.3 and 0.4 (Figure 11B). As effective diameter is taken in to account in PDI calculations, this increase in PDI may have been due to a combination of reduced MFNP size and decreased particle homogeneity in comparison to those produced with FEP tubing. An extended outlet length of laminar flow was hypothesized to reduce the MFNP PDI while also allowing for the addition of in-line crosslinking in future studies. When the outlet flow region was extended

from 15 cm to 100 cm (Table 2, Configuration E), the MFNP produced at 50 μL/min was measured at 13 nm, the smallest observed in the study. Nevertheless, PDI ranged between 0.3 and 0.4 similar to Configuration D, which suggests that a laminar flow quiescent zone did not reduce the PDI of the MFNPs. Figure 11C displays the size and PDI of each nanoparticle synthesized as a function of feed flow rate.

The two distinct ranges of nanoparticle sizes produced in this study each have unique applications. For cancer treatment applications, the well-documented enhanced permeability and retention (EPR) effect is the tendency of nm-scale particles to selectively accumulate within tumors due to leaky vasculature [90, 309]. Nanoparticles with diameters between 10 and 200 nm have been reported as optimal to deliver a therapeutic payload homogeneously throughout a tumor [90]. Other studies have utilized polymer-protein nanoparticles as bioscavengers and have even attached sub-30 nm nanoparticles to erythrocytes to extend circulation time *in vivo* [279, 310]. Consequently, the tunability and variety of size ranges of MFNPs synthesized with the millifluidic system may lead to advancements in scale-up for polymeric nanoparticles drug delivery systems.

Table 3: System configurations for millifluidic nanoparticle synthesis

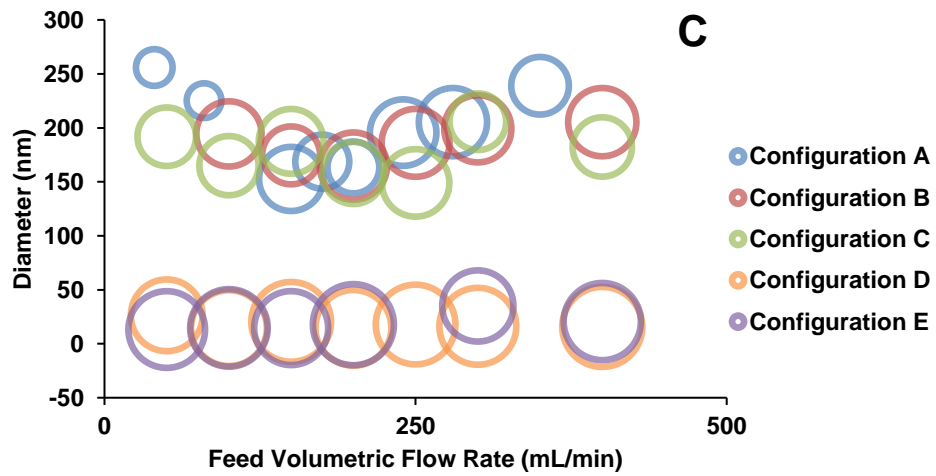| System configuration	Sonication power	Inlet length	Ultrasonication length	Outlet length	Tubing material
A	100 W	10 cm	75 cm	15 cm	FEP
B	110 W	10 cm	75 cm	15 cm	FEP
C	135 W	10 cm	75 cm	15 cm	FEP
D	135 W	10 cm	75 cm	15 cm	Silicone Rubber
E	135 W	10 cm	90 cm	100 cm	Silicone Rubber
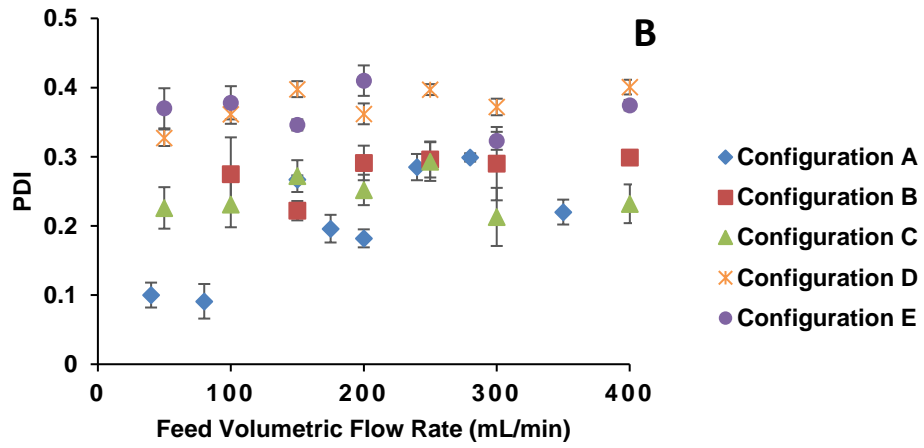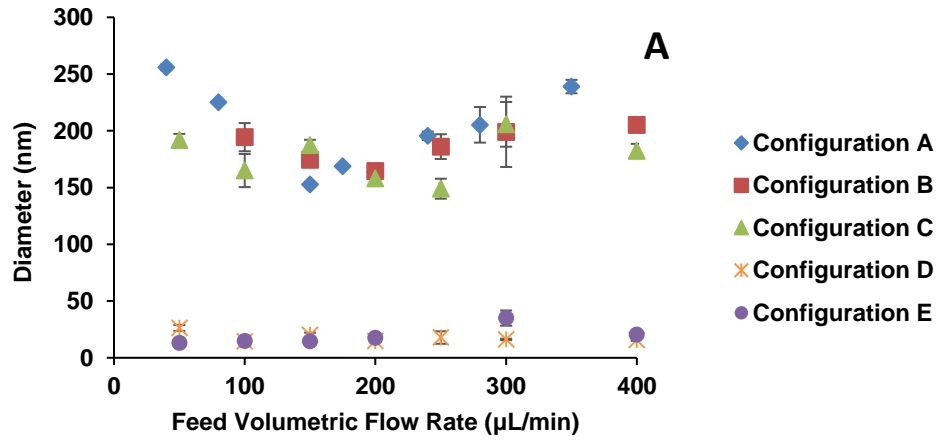
Figure 11: Diameter and polydispersity index (PDI) for nanoparticles synthesized using a millifluidic synthesis process. A) Nanoparticle diameter measured as a function of feed flow rate and ultrasonic power input. B) Nanoparticle PDI for each system configuration as a function of feed flow rate. PDI generally increased with increasing flow rate, and lower power inputs corresponded with lower PDI. C) Nanoparticle diameter (y-axis) and PDI (circle diameter) as a function of feed flow rate. Small nanoparticle diameter and high power input corresponded to higher PDI values, whereas lower power and larger sizes corresponded to lower PDI.

4.3.3. Nanoparticle microscopy and ζ-potential

The MFNPs selected for imaging were synthesized with Configuration E at a flow rate of 50 μL/min because these conditions displayed the smallest MFNP diameter. The MFNP size distribution was determined with scanning electron microscopy (SEM) (Figure 12). MFNPs displayed elliptical morphology and equivalent diameters ranged from 11 to 35 nm. ImageJ analysis of 436 particles from the SEM micrograph displayed a right-skewed distribution with a median particle equivalent diameter of 16.3 nm. Based on the size distribution, the concentration of the MFNPs was estimated as 1.1 μM with an average loading of 1.7 BSA per MFNP. In addition to SEM, transmission electron microscopy (TEM) was used to determine the morphology of the MFNPs. The dark rings correspond to reduced electron transmission whereas the centers display increased electron transmission, which is consistent with a core-shell morphology of a low-density center surrounded by a high-density coating. Furthermore, the morphology and size of MFNPs observed with TEM was consistent with that observed with SEM and DLS.
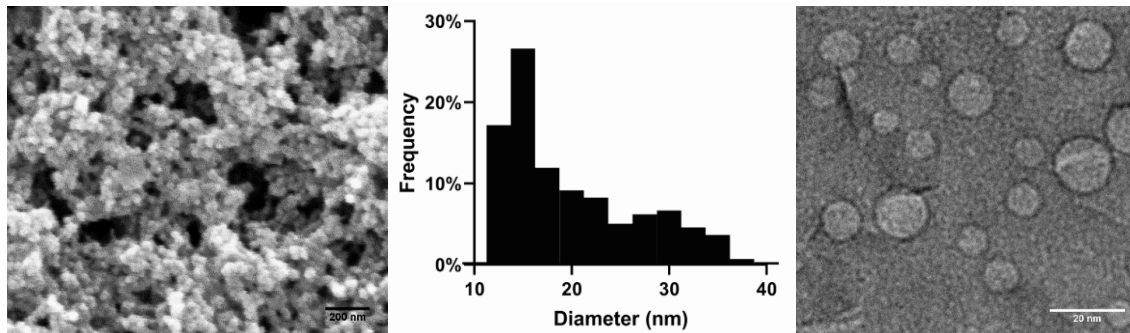
Figure 12: Electron microscopy of nanoparticles synthesized in a millifluidic process at a feed flow rate of 50 μL/min with a millifluidic process utilizing silicone rubber tubing and a 135W ultrasonic bath (Configuration E) The scanning electron micrograph (left) was analyzed using ImageJ to determine the size distribution (center) from 436 nanoparticles with a median diameter of 16.3 nm. The transmission electron micrograph (right) shows characteristic core-shell morphology with a high transmission center encompassed by a dark halo.

The ζ-potential of the MFNPs was measured using a ZetaPALS ζ-potential analyzer to determine the effect of encapsulation and crosslinking on MFNP surface charge. The MFNPs selected for ζ-potential analysis were those produced with Configuration E at feed flow rates of 50 and 300 μL/min. The MFNPs produced at 50 μL/min showed an average ζ-potential of 3.8±4.1 eV, while the MFNPs produced at 300 μL/min displayed a ζ-potential of 1.3±2.9 eV. As the ζ-potential of free BSA is -22 mV at pH 6.5 and -32 mV at pH 9.0 [280], this positive ζ-potential showed that the cationic amine groups and the hydrophilic PEG on the copolymer effectively shielded the charge of the encapsulated protein. This positive surface charge could be advantageous, as positively charged MFNPs display enhanced cellular uptake due to electrostatic interactions with negatively-charged glycosaminoglycans on cell membranes [281]. The near-neutral ζ-potential of the MFNPs may also reduce non-specific interactions with anionic serum proteins and affect the protein corona [129].

4.3.4. Nanoparticle protein encapsulation efficiency

The extent of protein encapsulation within PLL-g-PEG was determined using SDS-PAGE. As seen in Figure 13, both the free BSA and the non-crosslinked batch nanoparticle (Non-X NP) showed bands corresponding to the BSA monomer. In contrast, each of the MFNPs that had been crosslinked with glutaraldehyde displayed a thick dark band at the top of the gel resulting from the increased size and reduced relative migration when BSA was encapsulated within PLL-g-PEG. No MFNP showed a band matching that of free protein. These observations were identical to that of the well-characterized batch nanoparticle (BNP), for which it has been shown that free BSA band intensity increases with decreasing encapsulation efficiency [26]. Based on this evidence, the protein was fully encapsulated for all millifluidic system configurations and flow rates tested, which suggests that variations in size and PDI were not the result of variations in MFNP encapsulation efficiency.
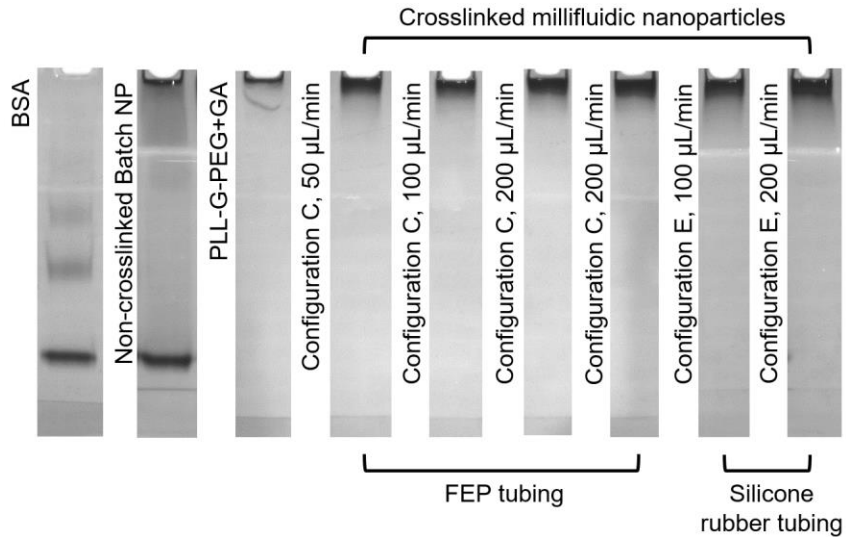
Figure 13: SDS-PAGE of nanoparticles synthesized through a millifluidic process and crosslinked with glutaraldehyde. All nanoparticles showed complete protein encapsulation.

4.3.5. Nanoparticle stability in the presence of chymotrypsin

The ability of the MFNPs to protect an encapsulated protein from degradation by proteases was confirmed using fluorescence spectroscopy. When incubated with 0.1 mg/mL chymotrypsin, both the MFNPs (Configuration E, 50µL/min) and the crosslinked BNPs protected the encapsulated protein significantly better than free DQBSA and non-crosslinked nanoparticles (Non-X NP) (Figure 14). The free DQBSA percentage of degraded protein increased quickly when exposed to the protease and reached 50% in 1.5 hours, while the Non-X NP showed a reduced degradation rate but followed closely behind the DQBSA. In contrast, the degradation of the crosslinked BNPs and MFNPs remained below 20% throughout the study.

The BNP and MFNP did display a small but significant difference in protein degradation after 32 hours of incubation. The MFNP showed slightly elevated degradation in comparison to the BNP. This evidence suggests that there was a difference in encapsulation between the batch and continuous processes, with the batch process producing nanoparticles with fewer surface-exposed proteins. Nevertheless, both synthesis processes produced polymer-protein nanoparticles that offer significant protection to the encapsulated protein in the presence of proteases.
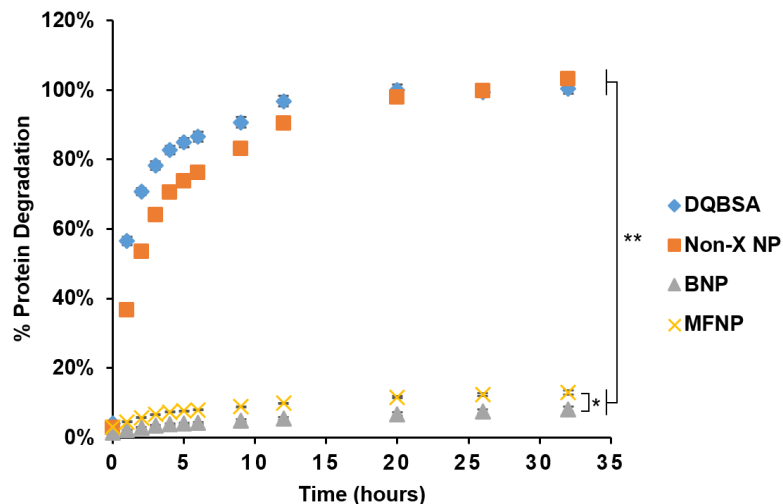
Figure 14: Stability of nanoparticles produced through a millifluidic process in the presence of chymotrypsin. The encapsulated protein (DQBSA) was labeled with a fluorescent probe such that it experienced self-quenching relievable by protease degradation. The non-crosslinked nanoparticle (Non-X NP) showed minimal protection for the encapsulated protein, closely following the curve of the free DQBSA. The glutaraldehyde-crosslinked nanoparticles produced through batch (BNP) and millifluidic (MFNP, Configuration E, 50 µL/min) processes showed strong protection for the encapsulated protein, though the BNPs protected the protein significantly better than the MFNPs did after 30 hours. * designates p-value < 0.01, ** designates p-value < 0.001.

4.3.6. Retention of esterolytic activity

Therapeutic protein delivery necessitates that the protein must retain its activity throughout the encapsulation and release processes. A prior study with butyrylcholinesterase suggested that PLL-g-PEG/protein complexing retained the activity of the encapsulated enzyme [285]. MFNP maintenance of encapsulated protein function was measured spectrophotometrically using the cleavage of 4-nitrophenyl octanoate. Hydrolysis of 4-nitrophenyl octanoate produces 4-nitrophenol, a product with an absorption peak at 410 nm. MFNPs synthesized with

Configuration E at both 50 and 300 µL/min were crosslinked with glutaraldehyde and compared to free BSA and BNPs in product concentration at various incubation times. Enzymatic binding and cleaving of the substrate was not hindered by encapsulation, which suggests encapsulation did not detrimentally affect protein function (Figure 15). Additionally, the MFNPs showed esterolytic activity similar to the BNPs. Both the MFNPs and the BNPs displayed higher product concentrations than free BSA at each time step, which is evidence that enzymatic activity was enhanced by the addition of the crosslinked copolymer. This is corroborated in previous studies and has been attributed to an increased localized substrate concentration within the nanoparticle leading to an increase in reaction rate [26, 286]. Furthermore, variation of the feed flow rate between 50 and 300 µL/min did not vary the amount by which the esterolytic activity was enhanced, suggesting that variations in time exposed to ultrasonication did not affect the enzymatic activity of the encapsulated protein.
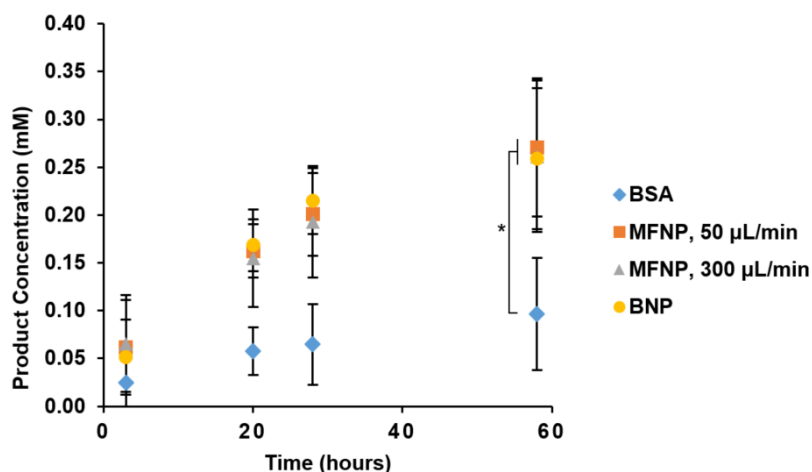
Figure 15: Retention of enzymatic activity for BSA nanoparticles encapsulated through batch and millifluidic processes. Free protein and nanoparticles were incubated with 4-nitrophenyl octanoate and the concentration of the esterolysis product 4-nitrophenol was measured spectrophotometrically. The enzymatic activity of nanoparticles produced with the millifluidic process (MFNP) matched that of the nanoparticles produced through a batch process (BNP). The

flow rate at which the nanoparticles were produced (50 or 300 μL/min) did not affect the

esterolytic activity of the encapsulated enzyme. All nanoparticles showed a higher product

concentration than the free protein at all times due to an enhanced localized substrate

concentration within the nanoparticle in comparison to that of the bulk fluid. After 58 hours of

incubation, each of the nanoparticles displayed significantly greater ($p < 0.01$) product

concentration that free BSA.

4.4. Conclusions

Polymeric nanoparticles were produced through a millifluidic process (MFNPs). Electrostatic

self-assembly was induced by ultrasonication within five system configurations. The resultant

nanoparticle diameter was a function of feed flow rate, ultrasonic power input, and tubing

material. MFNPs synthesized in FEP tubing ranged from 150 nm to 300 nm in diameter, whereas

MFNPs made with silicone rubber tubing displayed sizes below 30 nm. The MFNPs showed

complete protein encapsulation at all flow rates for all system configurations, maintained stability

in the presence of proteases, and retained the enzymatic activity of the encapsulated protein. The

millifluidic process this work presents is a favorable alternative to batch processes due to its

ability to rapidly synthesize polymer-protein nanoparticles with tunable properties. This work

could prove foundational to the development of continuous production processes for therapeutic

protein delivery systems, which would improve both nanoparticle consistency and throughput for

clinical applications.

CHAPTER V

CONCLUSIONS

The efficacy of current protein therapies is limited by delivery within the body. Previously, poly(L-lysine) was grafted with poly(ethylene glycol) and used to encapsulate a model protein. Herein, the effects of crosslinking poly(L-lysine)-grafted-poly(ethylene glycol) with redox responsive DTSSP were explored, with DTSSP crosslinking affecting particle size, polydispersity index, encapsulation efficiency, stability, and enzymatic activity. Through creation and characterization of a nanoparticle library, DTSSP NPs were observed to fully encapsulate bovine serum albumin, protect the encapsulated protein in a variety of conditions, and destabilize in a reductive environment.

Additionally, copolymer-protein nanoparticles were effectively formed through electrostatic self-assembly through a millifluidic process, which resulted in consistent nanoparticles with enhanced tunability and scalability over batch processes. The hydrodynamic diameter of the nanoparticles ranged from 13 to 300 nm and was dependent on feed flow rate, tubing material, and ultrasonic power input. The rapidly-formed millifluidic nanoparticles showed enzymatic activity comparable to nanoparticles produced through batch processes and protection for the encapsulated protein against proteolytic enzymes. Consequently, stimulus-responsive crosslinking and millifluidic synthesis show potential to improve the clinical relevance and medicinal efficacy of protein therapeutics.

REFERENCES

1. Usmani, S., et al., *THPdb: Database of FDA-approved peptide and protein therapeutics.*, in *PLoS ONE 12(7) e0181748*. 2017.
2. Alconcel, S.N.S., A.S. Baas, and H.D. Maynard, *FDA-approved poly(ethylene glycol)–protein conjugate drugs.* Polymer Chemistry, 2011. **2**(7).
3. Yin, L., C. Yuvienco, and J.K. Montclare, *Protein based therapeutic delivery agents: Contemporary developments and challenges.* Biomaterials, 2017. **134**: p. 91-116.
4. Zhao, H., et al., *Polymer-based nanoparticles for protein delivery: design, strategies and applications.* Journal of Materials Chemistry B, 2016. **4**(23): p. 4060-4071.
5. Dimitrov, D.S., *Therapeutic Proteins*, in *Therapeutic Proteins: Methods and Protocols*, V. Voynov and J.A. Caravella, Editors. 2012, Humana Press: Totowa, NJ. p. 1-26.
6. Rogers, K.e. and G. Gale, *The components of life from nucleic acids to carbohydrates*. 1st ed ed. 2011, New York: New York : Britannica Educational Pub. in association with Rosen Educational Services.
7. Roberts, C.J., *Therapeutic protein aggregation: mechanisms, design, and control.* Trends in Biotechnology, 2014. **32**(7): p. 372-380.
8. Sadasivuni, K.K., et al., *Polymer nanocomposites in biomedical engineering*. 2019: Cham, Switzerland : Springer.
9. Min, Y., et al., *Clinical Translation of Nanomedicine.* Chemical reviews, 2015. **115**(19): p. 11147.
10. Joshua D. Ramsey, N.H.F., *Cell-penetrating peptides transport therapeutics into cells.* Pharmacology & Therapeutics, 2015. **154**: p. 78-86.
11. Markiewicz, T., et al., *Protein Polymer-Based Nanoparticles: Fabrication and Medical Applications.* International Journal of Molecular Sciences, 2018. **19**(6): p. 1717.
12. Coester, C., P. Nayyar, and J. Samuel, *In vitro uptake of gelatin nanoparticles by murine dendritic cells and their intracellular localisation.* European Journal of Pharmaceutics and Biopharmaceutics, 2006. **62**(3): p. 306-314.
13. Webber, M., et al., *Supramolecular PEGylation of biopharmaceuticals.* Proceedings of the National Academy of Sciences, USA, 2016. **113**(50): p. 14189-14189.

14. Pathak, Y.V., *Surface modification of nanoparticles for targeted drug delivery*. 2019, Cham: Cham : Springer.

15. Csaba, N., A. SГЎnchez, and M.J. Alonso, *PLGA: Poloxamer and PLGA: Poloxamine blend nanostructures as carriers for nasal gene delivery*. Journal of Controlled Release, 2006. **113**(2): p. 164-172.

16. Lu, C. and M.W. Urban, *Stimuli-responsive polymer nano-science: Shape anisotropy, responsiveness, applications*. Progress in Polymer Science, 2018. **78**: p. 24-46.

17. Crucho, C.I.C., *Stimuli-Responsive Polymeric Nanoparticles for Nanomedicine*. 2015: Weinheim. p. 24-38.

18. Weiwei Gao, J.C., and Omid C. Farokhzad, *pH-responsive Nanoparticles for Drug Delivery*. Molecular Pharmaceuticals, 2010. **7**: p. 1913-1920.

19. Ssu-Ting Liu, H.-Y.T.-M., Jin-Jia Hu and Jeng-Shiung Jan, *Genipin cross-linked PEG-block-poly(L-lysine)/disulfide-based polymer complex micelles as fluorescent probes and pH-/redox-responsive drug vehicles*. Royal Society of Chemistry Advances, 2015. **5**: p. 87098–87107.

20. Yi-Xuan Zhang, Y.-F.C., Xuan-You Shen, Jin-Jia Hu, Jeng-Shiung Jan, *Reduction- and pH-Sensitive lipoic acid-modified Poly(L-lysine) and polypeptide/silica hybrid hydrogels/nanogels*. Polymer, 2015. **86**: p. 32-41.

21. Lee, S.-M., et al., *Nanoparticle-encapsulated P2X7 receptor antagonist in a pH-sensitive polymer as a potential local drug delivery system to acidic inflammatory environments*. Bioorganic & Medicinal Chemistry Letters, 2015. **25**(19): p. 4197-4202.

22. Huang, D., et al., *A novel technology using transscleral ultrasound to deliver protein loaded nanoparticles*. European Journal of Pharmaceutics and Biopharmaceutics, 2014. **88**(1): p. 104-115.

23. Tran, T.-T., et al., *Millifluidic synthesis of amorphous drug-polysaccharide nanoparticle complex with tunable size intended for supersaturating drug delivery applications*. European Journal of Pharmaceutics and Biopharmaceutics, 2017. **112**: p. 196-203.

24. Yang, J., et al., *FedвЂђbatch bioreactor process scaleвЂђup from 3вЂђL to 2,500вЂђL scale for monoclonal antibody production from cell culture*. Biotechnology and Bioengineering, 2007. **98**(1): p. 141-154.

25. Shuler, M.L., *Bioprocess engineering : basic concepts*. 2nd ed.. ed, ed. F. Kargi. 2002, Upper Saddle River, NJ: Upper Saddle River, NJ : Prentice Hall.

26. Flynn, N., et al., *Effect of cationic grafted copolymer structure on the encapsulation of bovine serum albumin*. Mater Sci Eng C Mater Biol Appl, 2016. **62**: p. 524-31.

27. Drews, J., *Drug Discovery: A Historical Perspective*. Science, 2000. **287**(5460): p. 1960.

28.   Fenton, O.S., et al., *Advances in Biomaterials for Drug Delivery.* Advanced Materials, 2018. **30**(29): p. 1705328.

29.   Tibbitt, M.W., J.E. Dahlman, and R. Langer, *Emerging Frontiers in Drug Delivery.* Journal of the American Chemical Society, 2016. **138**(3): p. 704-717.

30.   Kim, J.-M., et al., *Gene delivery platforms.* Biotechnology and Bioprocess Engineering, 2013. **18**(4): p. 637-647.

31.   Yu, M., et al., *Nanotechnology for protein delivery: Overview and perspectives.* Journal of Controlled Release, 2016. **240**: p. 24-37.

32.   Li, J., et al., *Strategies to release doxorubicin from doxorubicin delivery vehicles.* 2018. p. 9-26.

33.   Abbina, S. and A. Parambath, *14 - PEGylation and its alternatives: A summary*, in *Engineering of Biomaterials for Drug Delivery Systems*, A. Parambath, Editor. 2018, Woodhead Publishing. p. 363-376.

34.   Ganesh Kumar, C., Y. Poornachandra, and S. Pombala, *Chapter 1 - Therapeutic nanomaterials: from a drug delivery perspective*, in *Nanostructures for Drug Delivery*, E. Andronescu and A.M. Grumezescu, Editors. 2017, Elsevier. p. 1-61.

35.   Cao, J., et al., *Cellular internalization of doxorubicin loaded star-shaped micelles with hydrophilic zwitterionic sulfobetaine segments.* Biomaterials, 2014. **35**(15): p. 4517-4524.

36.   Chen, Y., et al., *Zwitterionic supramolecular prodrug nanoparticles based on host-guest interactions for intracellular drug delivery.* Polymer, 2016. **97**: p. 449-455.

37.   Walker, J.A., et al., *Antibody-Binding, Antifouling Surface Coatings Based on Recombinant Expression of Zwitterionic EK Peptides.* Langmuir, 2019. **35**(5): p. 1266-1272.

38.   Wang, Z., et al., *Development of zwitterionic polymer-based doxorubicin conjugates: Tuning the surface charge to prolong the circulation and reduce toxicity.* Langmuir, 2014. **30**(13): p. 3764-3774.

39.   Chatterjee, S. and T. Ooya, *Hydrophobic Nature of Methacrylate-POSS in Combination with 2-(Methacryloyloxy)ethyl Phosphorylcholine for Enhanced Solubility and Controlled Release of Paclitaxel.* Langmuir, 2019. **35**(5): p. 1404-1412.

40.   Vaidya , B., G.P. Agrawal, and S.P. Vyas, *Functionalized carriers for the improved delivery of plasminogen activators.* International Journal of Pharmaceutics, 2012. **424**: p. 1-11.

41.   Skubitz, K., *Paclitaxel*. 2012. p. 2755-2758.

42.   Li, F., et al., *Preparation and Characterization of Lipophilic Doxorubicin Pro-drug Micelles.* Journal of visualized experiments : JoVE, 2016(114): p. 54338.

43.   Lorusso, D., et al., *Patients' perception of chemotherapy side effects: Expectations, doctor–patient communication and impact on quality of life – An Italian survey.* European Journal of Cancer Care, 2017. **26**(2): p. n/a-n/a.

44.   Huang, H., et al., *pH-sensitive Au-BSA-DOX-FA nanocomposites for combined CT imaging and targeted drug delivery.* International Journal of Nanomedicine, 2017. **12**: p. 2829-2843.

45.   Thao, L.Q., et al., *Doxorubicin and paclitaxel co-bound lactosylated albumin nanoparticles having targetability to hepatocellular carcinoma.* Colloids and Surfaces B: Biointerfaces, 2017. **152**: p. 183-191.

46.   Obata, Y., S. Tajima, and S. Takeoka, *Evaluation of pH-responsive liposomes containing amino acid-based zwitterionic lipids for improving intracellular drug delivery in vitro and in vivo.* Journal of Controlled Release, 2010. **142**(2): p. 267-276.

47.   Huang, P., et al., *Zwitterionic nanoparticles constructed from bioreducible RAFT–ROP double head agent for shell shedding triggered intracellular drug delivery.* Acta Biomaterialia, 2016. **40**: p. 263-272.

48.   Zhao, L., et al., *pH triggered injectable amphiphilic hydrogel containing doxorubicin and paclitaxel.* International Journal of Pharmaceutics, 2011. **410**(1-2): p. 83-91.

49.   Dadsetan, M., et al., *A stimuli-responsive hydrogel for doxorubicin delivery.* Biomaterials, 2010. **31**(31): p. 8051-8062.

50.   Liu, Z., et al., *Shear-responsive injectable supramolecular hydrogel releasing doxorubicin loaded micelles with pH-sensitivity for local tumor chemotherapy.* International Journal of Pharmaceutics, 2017. **530**(1-2): p. 53-62.

51.   Brody, H., *Gene therapy.* Nature, 2018. **564**(7735): p. S5.

52.   El-Aneed, A., *An overview of current delivery systems in cancer gene therapy.* 2004. p. 1-14.

53.   Machida, C.A., *Viral vectors for gene therapy : methods and protocols.* 2003, Totowa, N.J.: Totowa, N.J. : Humana Press.

54.   Sharon, D. and A. Kamen, *Advancements in the design and scalable production of viral gene transfer vectors.* Biotechnology and Bioengineering, 2018. **115**(1): p. 25-40.

55.   MancheΓ±o-Corvo, P. and P. MartΓ-n-Duque, *Viral gene therapy.* Clinical and Translational Oncology, 2006. **8**(12): p. 858-867.

56.   Taira, K., K. Kataoka, and T. Niidome, *Non-viral gene therapy: Gene design and delivery.* 2005. 1-487.

57.   Sun, J., et al., *Grafting zwitterionic polymer chains onto PEI as a convenient strategy to enhance gene delivery performance.* Polymer Chemistry, 2013. **4**(24): p. 5810-5818.

58.   Tian, H., et al., *pH-responsive zwitterionic copolypeptides as charge conversional shielding system for gene carriers.* Journal of Controlled Release, 2014. **174**: p. 117-125.

59. Sun, J., et al., *Conjugation with betaine: a facile and effective approach to significant improvement of gene delivery properties of PEI.* Biomacromolecules, 2013. **14**(3): p. 728-736.

60. FernΓŸndez FernΓŸndez, E., et al., *Chitosan as a non-viral co-transfection system in a cystic fibrosis cell line.* International Journal of Pharmaceutics, 2016. **502**(1-2): p. 1-9.

61. Lu, H., et al., *Chitosan-Graft-Polyethylenimine/DNA Nanoparticles as Novel Non-Viral Gene Delivery Vectors Targeting Osteoarthritis.* PLoS One, 2014. **9**(1): p. e84703.

62. Nigatu, A.S., et al., *Effects of cell-penetrating peptides on transduction efficiency of PEGylated adenovirus.* Biomedicine & Pharmacotherapy, 2015. **71**: p. 153-160.

63. Wu, P., et al., *Non-viral gene delivery systems for tissue repair and regeneration.* Journal of Translational Medicine, 2018. **16**(1): p. 29.

64. Singarapu, K., I. Pal, and J.D. Ramsey, *Polyethylene glycolвЂ"grafted polyethylenimine used to enhance adenovirus gene delivery.* Journal of Biomedical Materials Research Part A, 2013. **101**(7): p. 1857-1864.

65. DeLuca, H.F., *Biochemistry*. 1st ed. 1979.. ed, ed. H.E. Paaren, et al. 1979, Berlin; New York: Berlin, Heidelberg : Springer Berlin Heidelberg : Imprint: Springer.

66. Dimitrov, A.S., *Therapeutic antibodies : methods and protocols*. 2009, New York, NY: New York, NY : Humana.

67. Voynov, V. and J.A. Caravella, *Therapeutic proteins : methods and protocols*. 2nd ed.. ed. 2012, New York: New York : Humana Press : Springer.

68. Cao, Z. and S. Jiang, *Super-hydrophilic zwitterionic poly(carboxybetaine) and amphiphilic non-ionic poly(ethylene glycol) for stealth nanoparticles.* Nano Today, 2012. **7**(5): p. 404-413.

69. Christian, D.A., et al., *Polymersome carriers: From self-assembly to siRNA and protein therapeutics.* European Journal of Pharmaceutics and Biopharmaceutics, 2009. **71**(3): p. 463-474.

70. Chou, Y.-N., et al., *Ultra-low fouling and high antibody loading zwitterionic hydrogel coatings for sensing and detection in complex media.* Acta Biomaterialia, 2016. **40**: p. 31-37.

71. Wu, J., et al., *Protein diffusion characteristics in the hydrogels of poly(ethylene glycol) and zwitterionic poly(sulfobetaine methacrylate) (pSBMA).* Acta Biomaterialia, 2016. **40**: p. 172-181.

72. Shan, W., et al., *Enhanced oral delivery of protein drugs using zwitterion-functionalized nanoparticles to overcome both the diffusion and absorption barriers.* ACS applied materials & interfaces, 2016. **8**(38): p. 25444-25453.

73. Zarzar, J., et al., *Impact of polymer geometry on the interactions of protein-PEG conjugates.* Biophysical Chemistry, 2018. **236**: p. 22-30.

74.   Veronese, F.M. and SpringerLink, *PEGylated protein drugs : basic science and clinical applications*. 2009, Basel; Boston: Basel; Boston : BirkhaM€user.

75.   Hossain, M.T., et al., *Crystal Structure of Uricase from Arthrobacter globiformis*. 2005: http://www.rcsb.org/structure/1VAX.

76.   Pawar, N., K. Rawat, and H.B. Bohidar, *Self-assembly of synthetic liposome-like curcumin nanoparticles.* RSC Advances, 2016. **6**(77): p. 73677-73682.

77.   Cao, Z., L. Zhang, and S. Jiang, *Superhydrophilic zwitterionic polymers stabilize liposomes.* Langmuir, 2012. **28**(31): p. 11625-11632.

78.   Liu, J., et al., *CO 2 gas induced drug release from pH-sensitive liposome to circumvent doxorubicin resistant cells.* Chemical Communications, 2012. **48**(40): p. 4869-4871.

79.   Mo, R., et al., *Intracellular delivery and antitumor effects of pH-sensitive liposomes based on zwitterionic oligopeptide lipids.* Biomaterials, 2013. **34**(11): p. 2773-2786.

80.   Lindner, L.H., et al., *Dual role of hexadecylphosphocholine (miltefosine) in thermosensitive liposomes: Active ingredient and mediator of drug release.* Journal of Controlled Release, 2008. **125**(2): p. 112-120.

81.   Zhu, L., et al., *Targeted delivery of methotrexate to skeletal muscular tissue by thermosensitive magnetoliposomes.* International Journal of Pharmaceutics, 2009. **370**(1): p. 136-143.

82.   Ibsen, S., et al., *A novel nested liposome drug delivery vehicle capable of ultrasound triggered release of its payload.* Journal of Controlled Release, 2011. **155**(3): p. 358-366.

83.   Li, J., et al., *Photoinduced drug release from complexes of liposome and fluorescent silver nanoparticles.* RSC Advances, 2014. **4**(19): p. 9476-9479.

84.   Qiu, D. and X. An, *Controllable release from magnetoliposomes by magnetic stimulation and thermal stimulation.* Colloids and Surfaces B: Biointerfaces, 2013. **104**: p. 326-329.

85.   Lin, D., et al., *Stimulusеђђ Responsive Hydrogel for Ophthalmic Drug Delivery.* Macromolecular Bioscience, 2019. **19**(6): p. n/a-n/a.

86.   Das, D., et al., *Stimulus-Responsive, Biodegradable, Biocompatible, Covalently Cross-Linked Hydrogel Based on Dextrin and Poly(N-isopropylacrylamide) for in Vitro/in Vivo Controlled Drug Release.* ACS applied materials & interfaces, 2015. **7**(26): p. 14338.

87.   Kim, D., et al., *Microfluidic synthesis of pH-sensitive multiamine hydrogel microparticles and release characterization of anticancer drug of doxorubicin (Dox).* Journal of Drug Delivery Science and Technology, 2014. **24**(5): p. 464-468.

88.   Ji, W., et al., *A Redoxеђђ Responsive Supramolecular Hydrogel for Controllable Dye Release.* Macromolecular Chemistry and Physics, 2015. **216**(19): p. 1945-1951.

89. Hu, C.-C., et al., *Thermo-responsive hydrogel as an anti-VEGF drug delivery system to inhibit retinal angiogenesis in Rex rabbits.* Technology and health care : official journal of the European Society for Engineering and Medicine, 2019. **27**(S1): p. 153.

90. Kobayashi, H., R. Watanabe, and P.L. Choyke, *Improving conventional enhanced permeability and retention (EPR) effects: what is the appropriate target?* Theranostics, 2013. **4**(1): p. 81.

91. McNeil, S.E., *Characterization of nanoparticles intended for drug delivery.* 2011, New York, N.Y.: New York, N.Y. : Humana Press.

92. Haydar, A. and N. Jana, *Plasmonic photocatalysis: complete degradation of bisphenol A by a gold nanoparticleвЂ"reduced graphene oxide composite under visible light.* Photochemical & Photobiological Sciences, 2018. **17**(5): p. 628-637.

93. Chakraborty, S., et al., *Bio-mediated silver nanoparticle synthesis: mechanism and microbial inactivation.* Toxicological & Environmental Chemistry, 2017. **99**(3): p. 434-447.

94. Hyeon, T., *Chemical synthesis of magnetic nanoparticles.* Chemical Communications, 2003(8): p. 927-934.

95. Mornet, S., et al., *Magnetic nanoparticle design for medical applications.* Progress in Solid State Chemistry, 2006. **34**(2): p. 237-247.

96. Lu, A.-H., E.L. Salabas, and F. Schüth, *Magnetic Nanoparticles: Synthesis, Protection, Functionalization, and Application.* Angewandte Chemie International Edition, 2007. **46**(8): p. 1222-1244.

97. Peng, L.-H., et al., *TAT conjugated cationic noble metal nanoparticles for gene delivery to epidermal stem cells.* Biomaterials, 2014. **35**(21): p. 5605-5618.

98. Agotegaray, M.A., *Silica-coated magnetic nanoparticles : an insight into targeted drug delivery and toxicology*, ed. V.L. Lassalle. 2017: Cham, Switzerland : Springer.

99. Tietze, R., et al., *Magnetic nanoparticle-based drug delivery for cancer therapy.* Biochemical and Biophysical Research Communications, 2015. **468**(3): p. 463-470.

100. Lee, I.-H., et al., *Imageable Antigen-Presenting Gold Nanoparticle Vaccines for Effective Cancer Immunotherapy In Vivo.* Angewandte Chemie International Edition, 2012. **51**(35): p. 8800-8805.

101. Chen, J., et al., *Advances in nanomaterials for photodynamic therapy applications: Status and challenges.* Biomaterials, 2020. **237**: p. 119827.

102. Du, B., et al., *Anionic Lipid, pH-Sensitive liposome-gold nanoparticle hybrids for gene delivery - Quantitative research of the mechanism.* Small, 2015. **11**(19): p. 2333-2340.

103. Dutta, S., et al., *Polymer grafted magnetic nanoparticles for delivery of anticancer drug at lower pH and elevated temperature.* Journal of Colloid And Interface Science, 2016. **467**: p. 70-80.

104. Chao, X., et al., *A novel magnetic nanoparticle drug carrier for enhanced cancer chemotherapy.* PloS one, 2012. **7**(10): p. e40388.

105. Encabo-Berzosa, M.M., et al., *Polymer functionalized gold nanoparticles as nonviral gene delivery reagents.* The journal of gene medicine, 2017. **19**(6-7).

106. Pucek, A., A. Lewińska, and K.A. Wilk, *Co-encapsulating solid lipid nanoparticles for multifunctional therapeutics: Preparation and characterization.* Colloids and Surfaces A: Physicochemical and Engineering Aspects, 2016. **510**: p. 11-21.

107. Permana, A.D., et al., *Solid lipid nanoparticle-based dissolving microneedles: A promising intradermal lymph targeting drug delivery system with potential for enhanced treatment of lymphatic filariasis.* Journal of Controlled Release, 2019. **316**: p. 34-52.

108. Das, S. and A. Chaudhury, *Recent Advances in Lipid Nanoparticle Formulations with Solid Matrix for Oral Drug Delivery.* AAPS PharmSciTech, 2011. **12**(1): p. 62-76.

109. Baek, J.-S. and C.-W. Cho, *Surface modification of solid lipid nanoparticles for oral delivery of curcumin: Improvement of bioavailability through enhanced cellular uptake, and lymphatic uptake.* European Journal of Pharmaceutics and Biopharmaceutics, 2017. **117**: p. 132-140.

110. Vallet-Regi, M., et al., *A new property of MCM-41: Drug delivery system.* Chemistry of Materials, 2001. **13**(2): p. 308-311.

111. Manzano, M. and M. Vallet-RegΓ-, *Mesoporous Silica Nanoparticles for Drug Delivery.* Advanced Functional Materials, 2019. **30**(2): p. <xocs:firstpage xmlns:xocs=""/>.

112. Tarn, D., et al., *Mesoporous Silica Nanoparticle Nanocarriers: Biofunctionality and Biocompatibility.* Accounts of Chemical Research, 2013. **46**(3): p. 792-801.

113. Argyo, C., et al., *Multifunctional Mesoporous Silica Nanoparticles as a Universal Platform for Drug Delivery.* Chemistry of Materials, 2014. **26**(1): p. 435-451.

114. Izquierdo-Barba, I., et al., *Tissue regeneration: A new property of mesoporous materials.* Solid State Sciences, 2005. **7**(8): p. 983-989.

115. Ruiz-Hernández, E., A. Baeza, and M. Vallet-Regí, *Smart Drug Delivery through DNA/Magnetic Nanoparticle Gates.* ACS Nano, 2011. **5**(2): p. 1259-1266.

116. Lai, C.-Y., et al., *A Mesoporous Silica Nanosphere-Based Carrier System with Chemically Removable CdS Nanoparticle Caps for Stimuli-Responsive Controlled Release of Neurotransmitters and Drug Molecules.* Journal of the American Chemical Society, 2003. **125**(15): p. 4451-4459.

117. Lu, J., et al., *Mesoporous Silica Nanoparticles as a Delivery System for Hydrophobic Anticancer Drugs.* Small, 2007. **3**(8): p. 1341-1346.

118. Chaiyasan, W., S.P. Srinivas, and W. Tiyaboonchai, *Crosslinked chitosan-dextran sulfate nanoparticle for improved topical ocular drug delivery.* Molecular vision, 2015. **21**: p. 1224.

119.   Pokharkar, V., V. Patil, and L. Mandpe, *Engineering of polymer-surfactant nanoparticles of doxycycline hydrochloride for ocular drug delivery.* Drug Delivery, 2015. **22**(7): p. 955-968.

120.   Beck-Broichsitter, M., et al., *Polymer Nanoparticle-Based Controlled Pulmonary Drug Delivery*, in *Drug Delivery System*, K.K. Jain, Editor. 2014, Springer New York: New York, NY. p. 133-145.

121.   Cheng, R., et al., *Glutathione-responsive nano-vehicles as a promising platform for targeted intracellular drug and gene delivery.* J Control Release, 2011. **152**(1): p. 2-12.

122.   Colson, Y.L. and M.W. Grinstaff, *Biologically Responsive Polymeric Nanoparticles for Drug Delivery.* Advanced Materials, 2012. **24**(28): p. 3878-3886.

123.   Dorresteijn, R., et al., *Drug Delivery: PolylactideвЂђ block вЂђPolypeptideвЂђ block вЂђPolylactide Copolymer Nanoparticles with Tunable Cleavage and Controlled Drug Release (Adv. Funct. Mater. 26/2014.* Advanced Functional Materials, 2014. **24**(26): p. 4025-4025.

124.   Yang, Y., et al., *Biodegradable and amphiphilic block copolymerвЂ"doxorubicin conjugate as polymeric nanoscale drug delivery vehicle for breast cancer therapy.* Biomaterials, 2013. **34**(33): p. 8430-8443.

125.   Zhang, S., et al., *Synthesis and Evaluation of Clickable Block Copolymers for Targeted Nanoparticle Drug Delivery.* Molecular Pharmaceutics, 2012. **9**(8): p. 2228-2236-2228-2236.

126.   Kaamyabi, S., D. Habibi, and M.M. Amini, *Preparation and characterization of the pH and thermosensitive magnetic molecular imprinted nanoparticle polymer for the cancer drug delivery.* Bioorganic & Medicinal Chemistry Letters, 2016. **26**(9): p. 2349-2354.

127.   MГјller, J., et al., *Coating nanoparticles with tunable surfactants facilitates control over the protein corona.* Biomaterials, 2017. **115**: p. 1-8.

128.   Cedervall, T., et al., *Understanding the nanoparticle–protein corona using methods to quantify exchange rates and affinities of proteins for nanoparticles.* Proceedings of the National Academy of Sciences, 2007. **104**(7): p. 2050.

129.   Lundqvist, M., et al., *The evolution of the protein corona around nanoparticles: A test study.* ACS Nano, 2011. **5**(9): p. 7503-7509.

130.   Schöttler, S., et al., *Protein adsorption is required for stealth effect of poly(ethylene glycol)- and poly(phosphoester)-coated nanocarriers.* Nature Nanotechnology, 2016. **11**(4): p. 372-377.

131.   Mirshafiee, V., et al., *Impact of protein pre-coating on the protein corona composition and nanoparticle cellular uptake.* Biomaterials, 2016. **75**: p. 295-304.

132.   Müller, J., et al., *Coating nanoparticles with tunable surfactants facilitates control over the protein corona.* Biomaterials, 2017. **115**: p. 1-8.

133. Ishihara, K., et al., *The unique hydration state of poly(2-methacryloyloxyethyl phosphorylcholine).* Journal of Biomaterials Science, Polymer Edition, 2017. **28**(10-12): p. 884-899.

134. Chen, S., et al., *Surface hydration: Principles and applications toward low-fouling/nonfouling biomaterials.* Polymer, 2010. **51**(23): p. 5283-5293.

135. Leng, C., et al., *Probing the Surface Hydration of Nonfouling Zwitterionic and PEG Materials in Contact with Proteins.* ACS Applied Materials & Interfaces, 2015. **7**(30): p. 16881-16888.

136. Dai, J., et al., *Polyethylenimine-grafted copolymer of poly(l-lysine) and poly(ethylene glycol) for gene delivery.* Biomaterials, 2011. **32**(6): p. 1694.

137. Levine, P.M., et al., *Intrinsic bioconjugation for site-specific protein PEGylation at N-terminal serine.* Chemical Communications, 2014. **50**(52): p. 6909-6912.

138. Keefe, A.J. and S. Jiang, *Poly (zwitterionic) protein conjugates offer increased stability without sacrificing binding affinity or bioactivity.* Nature chemistry, 2012. **4**(1): p. 59.

139. Armstrong, J.K., et al., *Antibody against poly(ethylene glycol) adversely affects PEG-asparaginase therapy in acute lymphoblastic leukemia patients.* Cancer, 2007. **110**(1): p. 103.

140. Grenier, P., et al., *Anti-polyethylene glycol antibodies alter the protein corona deposited on nanoparticles and the physiological pathways regulating their fate in vivo.* Journal of Controlled Release, 2018. **287**: p. 121-131.

141. Cai, M., et al., *In vitro and in vivo anti-tumor efficiency comparison of phosphorylcholine micelles with PEG micelles.* Colloids and Surfaces B: Biointerfaces, 2017. **157**: p. 268-279.

142. Xiao, W., et al., *Prolonged in vivo circulation time by zwitterionic modification of magnetite nanoparticles for blood pool contrast agents.* Contrast Media and Molecular Imaging, 2012. **7**(3): p. 320-327.

143. Li, L., et al., *Zwitterionic shielded polymeric prodrug with folate-targeting and pH responsiveness for drug delivery.* Journal of Materials Chemistry B, 2019. **7**(5): p. 786-795.

144. Zhang, P., et al., *Zwitterionic gel encapsulation promotes protein stability, enhances pharmacokinetics, and reduces immunogenicity.* Proceedings of the National Academy of Sciences, 2015. **112**(39): p. 12046-12051.

145. Miller, J.B., et al., *Nonвʕ̵Viral CRISPR/Cas Gene Editing In Vitro and In Vivo Enabled by Synthetic Nanoparticle Coвʕ̵Delivery of Cas9 mRNA and sgRNA.* Angewandte Chemie International Edition, 2017. **56**(4): p. 1059-1063.

146. Kato, T., et al., *Adsorption of sulfobetaine polyampholyte on silica surfaces from aqueous salt solutions.* Langmuir, 1999. **15**(12): p. 4302-4305.

147. Kawata, Y., S. Kozuka, and S.-i. Yusa, *Thermo-Responsive Behavior of Amphoteric Diblock Copolymers Bearing Sulfonate and Quaternary Amino Pendant Groups.* Langmuir, 2019. **35**(5): p. 1458-1464.

148. Kim, D., H. Matsuoka, and Y. Saruwatari, *Synthesis and Stimuli Responsivity of Diblock Copolymers Composed of Sulfobetaine and Ionic Blocks: Influence of the Block Ratio.* Langmuir, 2019. **35**(5): p. 1590-1597.

149. Tu, Q., et al., *Synthesis of polyethylene glycol- and sulfobetaine-conjugated zwitterionic poly(l-lactide) and assay of its antifouling properties.* Colloids and Surfaces B: Biointerfaces, 2013. **102**: p. 331-340.

150. Viklund, C. and K. Irgum, *Synthesis of porous zwitterionic sulfobetaine monoliths and characterization of their interaction with proteins.* Macromolecules, 2000. **33**(7): p. 2539-2544.

151. Vuillard, L., T. Rabilloud, and M.E. Goldberg, *Interactions of non-detergent sulfobetaines with early folding intermediates facilitate in vitro protein renaturation.* European Journal of Biochemistry, 1998. **256**(1): p. 128-135.

152. Wangkanont, K., K.T. Forest, and L.L. Kiessling, *The non-detergent sulfobetaine-201 acts as a pharmacological chaperone to promote folding and crystallization of the type II TGF-β receptor extracellular domain.* Protein Expression and Purification, 2015. **115**: p. 19-25.

153. Wu, J., et al., *Sulfated zwitterionic poly(sulfobetaine methacrylate) hydrogels promote complete skin regeneration.* Acta Biomaterialia, 2018. **71**: p. 293-305.

154. Zhang, Z., et al., *Surface grafted sulfobetaine polymers via atom transfer radical polymerization as superlow fouling coatings.* Journal of Physical Chemistry B, 2006. **110**(22): p. 10799-10804.

155. Carr, L.R., H. Xue, and S. Jiang, *Functionalizable and nonfouling zwitterionic carboxybetaine hydrogels with a carboxybetaine dimethacrylate crosslinker.* Biomaterials, 2011. **32**(4): p. 961-968.

156. Vasantha, V.A., et al., *Reversible Photo- and Thermoresponsive, Self-Assembling Azobenzene Containing Zwitterionic Polymers.* Langmuir, 2019. **35**(5): p. 1465-1474.

157. Chien, H.W., W.B. Tsai, and S. Jiang, *Direct cell encapsulation in biodegradable and functionalizable carboxybetaine hydrogels.* Biomaterials, 2012. **33**(23): p. 5706-5712.

158. Huynh, V., et al., *Influence of Hydrophobic Cross-Linkers on Carboxybetaine Copolymer Stimuli Response and Hydrogel Biological Properties.* Langmuir, 2019. **35**(5): p. 1631-1641.

159. Izumrudov, V.A., et al., *Interpolyelectrolyte reactions in solutions of polycarboxybetaines.* Journal of Physical Chemistry B, 2003. **107**(32): p. 7982-7986.

160. Tsvetkov, N.V., et al., *Macromolecules of polycarboxybetaine poly(4-N,N-diallyl-N-methylammonio) butanoate: Synthesis and molecular characteristics.* Polymer, 2017. **122**: p. 34-44.

161. Yang, W., et al., *Functionalizable and ultra stable nanoparticles coated with zwitterionic poly(carboxybetaine) in undiluted blood serum.* Biomaterials, 2009. **30**(29): p. 5617-5621.

162. Zhang, Z., S. Chen, and S. Jiang, *Dual-functional biomimetic materials: Nonfouling poly(carboxybetaine) with active functional groups for protein immobilization.* Biomacromolecules, 2006. **7**(12): p. 3311-3315.

163. Zhang, Z., et al., *Nonfouling behavior of polycarboxybetaine-grafted surfaces: Structural and environmental effects.* Biomacromolecules, 2008. **9**(10): p. 2686-2692.

164. Zhao, G., X. Dong, and Y. Sun, *Self-Assembled Curcumin–Poly(carboxybetaine methacrylate) Conjugates: Potent Nano-Inhibitors against Amyloid β-Protein Fibrillogenesis and Cytotoxicity.* Langmuir, 2019. **35**(5): p. 1846-1857.

165. Kyomoto, M., et al., *Hydrated Phospholipid Polymer Gel-Like Layer for Increased Durability of Orthopedic Bearing Surfaces.* Langmuir, 2019. **35**(5): p. 1954-1963.

166. Ishihara, K. and Y. Iwasaki, *Reduced protein adsorption on novel phospholipid polymers.* Journal of Biomaterials Applications, 1998. **13**(2): p. 111-127.

167. Ishihara, K., et al., *Why do phospholipid polymers reduce protein adsorption?* Journal of Biomedical Materials Research, 1998. **39**(2): p. 323-330.

168. Ishihara, K., T. Ueda, and N. Nakabayashi, *Preparation of phospholipid polylners and their properties as polymer hydrogel membranes.* Polymer Journal, 1990. **22**(5): p. 355-360.

169. Nakaya, T. and Y.J. Li, *Phospholipid polymers.* Progress in Polymer Science (Oxford), 1999. **24**(1): p. 143-181.

170. Tanaka, M. and Y. Iwasaki, *Photo-assisted generation of phospholipid polymer substrates for regiospecific protein conjugation and control of cell adhesion.* Acta Biomaterialia, 2016. **40**: p. 54-61.

171. Allen, T.M., *Ligand-targeted therapeutics in anticancer therapy.* Nature Reviews Cancer, 2002. **2**(10): p. 750-763.

172. Attia, M.F., et al., *An overview of active and passive targeting strategies to improve the nanocarriers efficiency to tumour sites.* Journal of Pharmacy and Pharmacology, 2019. **71**(8): p. 1185-1198.

173. Patel, J.K. and A.P. Patel, *Passive Targeting of Nanoparticles to Cancer*, in *Surface Modification of Nanoparticles for Targeted Drug Delivery*, Y.V. Pathak, Editor. 2019, Springer International Publishing: Cham. p. 125-143.

174. Stapleton, S., et al., *A mathematical model of the enhanced permeability and retention effect for liposome transport in solid tumors.* PloS one, 2013. **8**(12): p. e81157.

175. Nakamura, Y., et al., *Nanodrug Delivery: Is the Enhanced Permeability and Retention Effect Sufficient for Curing Cancer?* Bioconjugate Chemistry, 2016. **27**(10): p. 2225-2238.

176.   Ou, H., et al., *Surface-adaptive zwitterionic nanoparticles for prolonged blood circulation time and enhanced cellular uptake in tumor cells.* Acta Biomaterialia, 2018. **65**: p. 339-348.

177.   Qin, Z., et al., *Mixed-Charged Zwitterionic Polymeric Micelles for Tumor Acidic Environment Responsive Intracellular Drug Delivery.* Langmuir, 2019. **35**(5): p. 1242-1248.

178.   Aston, W.J., et al., *A systematic investigation of the maximum tolerated dose of cytotoxic chemotherapy with and without supportive care in mice.* BMC cancer, 2017. **17**(1): p. 684-684.

179.   Li, S., et al., *ROS-Response-Induced Zwitterionic Dendrimer for Gene Delivery.* Langmuir, 2019. **35**(5): p. 1613-1620.

180.   Wen, Y., Z. Zhang, and J. Li, *Highly Efficient Multifunctional Supramolecular Gene Carrier System Self-Assembled from Redox-Sensitive and Zwitterionic Polymer Blocks.* Advanced Functional Materials, 2014. **24**(25): p. 3874-3884.

181.   Liang, J.F., et al., *ATTEMPTS: a heparin/protamine-based prodrug approach for delivery of thrombolytic drugs.* Journal of controlled release : official journal of the Controlled Release Society, 2001. **72**(1-3): p. 145-156.

182.   Park, Y.-J., et al., *ATTEMPTS: a heparin /protamine-based triggered release system for the delivery of enzyme drugs without associated side-effects* Advanced Drug Delivery Reviews, 2003. **55**: p. 251-265.

183.   Ye, J., et al., *15 years of ATTEMPTS: Amacromolecular drug delivery systembased on the CPP-mediated intracellular drug delivery and antibody targeting* Journal of Controlled Release, 2014. **205**: p. 58-69.

184.   Naik, S.S., et al., *Application of "ATTEMPTS" for drug delivery.* Journal of Controlled Release, 2005. **101**(1-3): p. 35-45.

185.   Zheyong Huang, Y.S., Zhiqing, M.L. Pang, Yerkintay Guliya, Yunli, and J.Q. Shen, Junbo Ge, *Fibrin-targeting delivery: a novel platform for cardiac regenerative medicine.* Journal of Cellular and Molecular Medicine, 2016. **20**.

186.   Klein, P.M., et al., *Folate receptor-directed orthogonal click-functionalization of siRNA lipopolyplexes for tumor cell killing inB vivo.* Biomaterials, 2018. **178**: p. 630-642.

187.   Absar, S., et al., *Thrombus-Targeted Nanocarrier Attenuates Bleeding Complications Associated with Conventional Thrombolytic Therapy.* Pharmaceutical Research, 2013. **30**(6): p. 1663-1676.

188.   Kanapathipillai, M., A. Brock, and D.E. Ingber, *Nanoparticle targeting of anti-cancer drugs that alter intracellular signaling or influence the tumor microenvironment.* Advanced Drug Delivery Reviews, 2014. **79-80**: p. 107-118.

189.   Nomoto, T. and N. Nishiyama, *Photodynamic Therapy*, in *Photochemistry for Biomedical Applications: From Device Fabrication to Diagnosis and Therapy*, Y. Ito, Editor. 2018, Springer Singapore: Singapore. p. 301-313.

190. Hua, X., et al., *Construction of thrombus-targeted microbubbles carrying tissue plasminogen activator and their in vitro thrombolysis efficacy: a primary research.* Journal of Thrombosis and Thrombolysis, 2010. **30**(1): p. 29-35.

191. Snipstad, S., et al., *Ultrasound-mediated delivery and distribution of polymeric nanoparticles in the normal brain parenchyma of a metastatic brain tumour model.* PLoS One, 2018. **13**(1): p. e0191102.

192. Sun, T., et al., *Closed-loop control of targeted ultrasound drug delivery across the blood-brain/tumor barriers in a rat glioma model.* Proceedings of the National Academy of Sciences of the United States of America, 2017. **114**(48): p. E10281.

193. Wan, Q., et al., *Self-assembled magnetic theranostic nanoparticles for highly sensitive MRI of minicircle DNA delivery.* Nanoscale, 2012. **5**(2): p. 744-752.

194. Liu, X.L., et al., *Synthesis of Ferromagnetic Fe0.6Mn0.4O Nanoflowers as a New Class of Magnetic Theranostic Platform for In Vivo T1ꞵT2 Dualꞵ Mode Magnetic Resonance Imaging and Magnetic Hyperthermia Therapy.* Advanced Healthcare Materials, 2016. **5**(16): p. 2092-2104.

195. Nosrati, H., et al., *Preparation and characterization of magnetic theranostic nanoparticles for curcumin delivery and evaluation as MRI contrast agent.* Applied Organometallic Chemistry, 2018. **32**(12): p. n/a-n/a.

196. Mody, V., et al., *Magnetic nanoparticle drug delivery systems for targeting tumor.* Applied Nanoscience, 2014. **4**(4): p. 385-392.

197. Brahimi-Horn, M.C., J. Chiche, and J. Pouysségur, *Hypoxia and cancer.* Journal of Molecular Medicine, 2007. **85**(12): p. 1301-1307.

198. Lee, H., et al., *Preliminary study on alginate/NIPAM hydrogel-based soft microrobot for controlled drug delivery using electromagnetic actuation and near-infrared stimulus.* Biomedical Microdevices, 2018. **20**(4): p. 1-9.

199. Nagasawa, Y., et al., *Influence of hydrophobicity of backbone polymer in thermo-responsive hydrogel with immobilized amine on cycle capacity for absorption and recovery of CO 2.* Polymers, 2019. **11**(6).

200. Wang, J., et al., *Fast responsive and morphologically robust thermo-responsive hydrogel nanofibres from poly(N -isopropylacrylamide) and POSS crosslinker.* Soft Matter, 2011. **7**(9): p. 4364-4369.

201. Lim, J., et al., *Temperature-Responsive Behavior of Double Hydrophilic Carboxy-Sulfobetaine Block Copolymers and Their Self-Assemblies in Water.* Langmuir, 2019. **35**(5): p. 1571-1582.

202. Xiao, L., et al., *Temperature responsive hydrogel with reactive nanoparticles.* Journal of Applied Polymer Science, 2013. **128**(3): p. 1804-1814.

203. Arotçaréna, M., et al., *Switching the Inside and the Outside of Aggregates of Water-Soluble Block Copolymers with Double Thermoresponsivity.* Journal of the American Chemical Society, 2002. **124**(14): p. 3787-3793.

204. Simona Mura, J.N.a.P.C., *Stimuli-responsive nanocarriers for drug delivery.* Nature Materials, 2013. **12**: p. 991-1003.

205. Xing, P. and Y. Zhao, *Supramolecular Vesicles for Stimulus-Responsive Drug Delivery.* Small Methods, 2018. **2**(4): p. 1700364.

206. Hou, J., et al., *A novel high drug loading mussel-inspired polydopamine hybrid nanoparticle as a pH-sensitive vehicle for drug delivery.* International Journal of Pharmaceutics, 2017. **533**(1): p. 73-83.

207. Izumrudov, V.A., et al., *Interpolyelectrolyte reactions in solutions of polycarboxybetaines.* The Journal of Physical Chemistry B, 2003. **107**(32): p. 7982-7986.

208. Jardim, B.V., et al., *Glutathione and glutathione peroxidase expression in breast cancer: an immunohistochemical and molecular study.* Oncology reports, 2013. **30**(3): p. 1119.

209. Ballatori, N., et al., *Glutathione dysregulation and the etiology and progression of human diseases.* Biological chemistry, 2009. **390**(3): p. 191-214.

210. Mutlu Agardan, N.B., C. Sarisozen, and V.P. Torchilin, *Redox-triggered intracellular siRNA delivery.* Chemical Communications, 2018. **54**(49): p. 6368-6371.

211. Xu, X., et al., *ROS-Responsive Polyprodrug Nanoparticles for Triggered Drug Delivery and Effective Cancer Therapy.* Advanced Materials, 2017. **29**(33): p. 1700141.

212. Wu, C., et al., *Redox-responsive supramolecular hydrogel based on 10-hydroxy camptothecin-peptide covalent conjugates with high loading capacity for drug delivery.* Materials Science & Engineering C, 2017. **76**: p. 196-202.

213. Liu, H., et al., *Facile fabrication of redox/pH dual stimuli responsive cellulose hydrogel.* Carbohydrate Polymers, 2017. **176**: p. 299-306.

214. K C, R.B., B. Thapa, and P. Xu, *pH and redox dual responsive nanoparticle for nuclear targeted drug delivery.* Molecular pharmaceutics, 2012. **9**(9): p. 2719.

215. Rasouli, M.R. and M. Tabrizian, *An ultra-rapid acoustic micromixer for synthesis of organic nanoparticles.* Lab on a Chip, 2019. **19**(19): p. 3316-3325.

216. Kim, Y., et al., *Mass Production and Size Control of Lipid–Polymer Hybrid Nanoparticles through Controlled Microvortices.* Nano Letters, 2012. **12**(7): p. 3587-3591.

217. Valencia, P.M., et al., *Microfluidic technologies for accelerating the clinical translation of nanoparticles.* Nature Nanotechnology, 2012. **7**(10): p. 623-629.

218. Martínez Rivas, C.J., et al., *Nanoprecipitation process: From encapsulation to drug delivery.* International Journal of Pharmaceutics, 2017. **532**(1): p. 66-81.

219. Roberts, E.J., et al., *Continuous Flow Methods of Fabricating Catalytically Active Metal Nanoparticles.* ACS applied materials & interfaces, 2019. **11**(31): p. 27479-27502.

220. Dong, B. and K. Hadinoto, *Direct comparison between millifluidic and bulk-mixing platform in the synthesis of amorphous drug-polysaccharide nanoparticle complex.* International Journal of Pharmaceutics, 2017. **523**(1): p. 42-51.

221. Lim, J.-M., et al., *Parallel microfluidic synthesis of size-tunable polymeric nanoparticles using 3D flow focusing towards in vivo study.* Nanomedicine: Nanotechnology, Biology, and Medicine, 2014. **10**(2): p. 401-409.
222. Pedro, M.V., et al., *Microfluidic technologies for accelerating the clinical translation of nanoparticles.* Nature Nanotechnology, 2012. **7**(10): p. 623.
223. Krishna, K.S., et al., *Lab-on-a-chip synthesis of inorganic nanomaterials and quantum dots for biomedical applications.* Advanced Drug Delivery Reviews, 2013. **65**(11-12): p. 1470-1495.
224. Akdas, T. and P. Reiss, *"Safer-by-design" synthesis of quantum dots in flow reactors.* Journal of Physics: Conference Series, 2019. **1323**: p. 012007.
225. Libi, S., et al., *Investigation on hemolytic effect of poly(lactic co-glycolic) acid nanoparticles synthesized using continuous flow and batch processes.* Nanotechnology Reviews, 2017. **6**(2).
226. Gottesman, R., et al., *Silver nanowires and nanoparticles from a millifluidic reactor: application to metal assisted silicon etching.* New Journal of Chemistry, 2012. **36**(12): p. 2456-2459.
227. Gu, T., et al., *Continuous Flow Synthesis of Superparamagnetic Nanoparticles in Reverse Miniemulsion Systems.* Colloid and Interface Science Communications, 2019. **28**: p. 1-4.
228. Gomez, C., et al., *Metallic bismuth nanoparticles: Towards a robust, productive and ultrasound assisted synthesis from batch to flow-continuous chemistry.* Ultrasonics Sonochemistry, 2019. **56**: p. 167-173.
229. Lee, C.-Y., et al., *Passive mixers in microfluidic systems: A review.* Chemical Engineering Journal, 2016. **288**: p. 146-160.
230. Wang, S., X. Huang, and C. Yang, *Mixing enhancement for high viscous fluids in a microfluidic chamber.* Lab on a Chip, 2011. **11**(12): p. 2081-2087.
231. Wang, Y., I. Nkurikiyimfura, and Z. Pan, *Sonochemical Synthesis of Magnetic Nanoparticles.* Chemical Engineering Communications, 2015. **202**(5): p. 616-621.
232. Bhanvase, B.A. and S.H. Sonawane, *Ultrasound assisted in situ emulsion polymerization for polymer nanocomposite: A review.* Chemical Engineering & Processing: Process Intensification, 2014. **85**: p. 86-107.
233. Huang, X., et al., *Ultrasound-enhanced Microfluidic Synthesis of Liposomes.* Anticancer Research, 2010. **30**(2): p. 463-466.
234. Poddar, M.K., et al., *Ultrasound-assisted synthesis and characterization of magnetite nanoparticles and poly(methyl methacrylate)/magnetite nanocomposites.* Ultrasonics Sonochemistry, 2018. **43**: p. 38-51.
235. Deshmukh, A.R., A. Gupta, and B.S. Kim, *Ultrasound Assisted Green Synthesis of Silver and Iron Oxide Nanoparticles Using Fenugreek Seed Extract and Their Enhanced Antibacterial and Antioxidant Activities.* BioMed research international, 2019. **2019**: p. 1714358.

236.   Manjamadha, V. and K. Muthukumar, *Ultrasound assisted green synthesis of silver nanoparticles using weed plant.* Bioprocess and Biosystems Engineering, 2016. **39**(3): p. 401-411.

237.   Dong, Z., et al., *Continuous Ultrasonic Reactors: Design, Mechanism and Application.* Materials (Basel), 2020. **13**(2).

238.   Wu, K. and S. Kuhn, *Strategies for solids handling in microreactors.* Chim. Oggi, 2014. **32**(3): p. 62.

239.   Fernandez, D.R. and S. Kuhn, *Synergy of Microfluidics and Ultrasound: Process Intensification Challenges and Opportunities.* Topics in current chemistry (Cham), 2016. **374**(5): p. 70-70.

240.   Fernandez Rivas, D., P. Cintas, and H.J.G.E. Gardeniers, *Merging microfluidics and sonochemistry: towards greener and more efficient micro-sono-reactors.* Chemical Communications, 2012. **48**(89): p. 10935-10947.

241.   Zhang, L., et al., *A polymeric nanocarrier with a tumor acidity-activatable arginine-rich (R9) peptide for enhanced drug delivery.* Biomaterials Science, 2020.

242.   Yanchun, W., et al., *Redox-responsive self-assembly PEG nanoparticle enhanced triptolide for efficient antitumor treatment.* Scientific Reports, 2018. **8**(1): p. 1-10.

243.   Xu, X., et al., *ROSâ€• Responsive Polyprodrug Nanoparticles for Triggered Drug Delivery and Effective Cancer Therapy.* Advanced Materials, 2017. **29**(33): p. n/a-n/a.

244.   Seo, B.-B., et al., *Sustained BMP-2 delivery and injectable bone regeneration using thermosensitive polymeric nanoparticle hydrogel bearing dual interactions with BMP-2.* Journal of Controlled Release, 2015. **209**: p. 67-76.

245.   Zhang, L., et al., *An acoustic/thermo-responsive hybrid system for advanced doxorubicin delivery in tumor treatment.* Biomaterials Science, 2020.

246.   Zhang, W., et al., *Doxorubicin-loaded magnetic nanoparticle clusters for chemo-photothermal treatment of the prostate cancer cell line PC3.* Biochemical and Biophysical Research Communications, 2015. **466**(2): p. 278-282.

247.   Yang, Y., et al., *Dual-stimuli responsive nanoparticle system for enhanced and targeted cancer therapy.* Journal of Controlled Release, 2017. **259**: p. e166-e167.

248.   Wu, D., et al., *Mesoporous polydopamine with built-in plasmonic core: Traceable and NIR triggered delivery of functional proteins.* Biomaterials, 2020. **238**: p. 119847.

249.   Zhang, C., et al., *Rod-based urchin-like hollow microspheres of Bi2S3: Facile synthesis, photo-controlled drug release for photoacoustic imaging and chemo-photothermal therapy of tumor ablation.* Biomaterials, 2020. **237**: p. 119835.

250.   Zhou, H., et al., *Intelligently thermoresponsive flower-like hollow nano-ruthenium system for sustained release of nerve growth factor to inhibit hyperphosphorylation of tau and neuronal damage for the treatment of Alzheimer's disease.* Biomaterials, 2020. **237**: p. 119822.

251. del Valle, A.C., et al., *NIR-cleavable drug adducts of gold nanostars for overcoming multidrug-resistant tumors.* Biomaterials Science, 2020.

252. Nguyen, H.X. and E.A. O'Rear, *Modified dextran, heparin-based triggered release microspheres for cardiovascular delivery of therapeutic drugs using protamine as a stimulus.* Journal of Microencapsulation, 2017. **34**(3): p. 299-307.

253. Dickinson, D.A., et al., *Human glutamate cysteine ligase gene regulation through the electrophile response element.* Free Radical Biology and Medicine, 2004. **37**(8): p. 1152-1159.

254. Dawson, N.J. and K.B. Storey, *Passive regeneration of glutathione: glutathione reductase regulation in the freeze-tolerant North American wood frog.* The Journal of experimental biology, 2017. **220**(17): p. 3162.

255. Zengin, E., et al., *Alterations in lipid peroxidation and antioxidant status in different types of intracranial tumors within their relative peritumoral tissues.* Clinical Neurology and Neurosurgery, 2009. **111**(4): p. 345-351.

256. Gamcsik, M.P., et al., *Glutathione levels in human tumors.* Biomarkers, 2012. **17**(8): p. 671-91.

257. Miran, T., et al., *Modulation of glutathione promotes apoptosis in triple-negative breast cancer cells.* FASEB journal : official publication of the Federation of American Societies for Experimental Biology, 2018. **32**(5): p. 2803.

258. de Campos Zuccari, D.P., et al., *890 The Prognostic Value of Glutathione (GSH) and Glutathione Peroxidase (GPX) in Breast Cancer.* European Journal of Cancer, 2012. **48**: p. S215-S215.

259. Malik, S.S., N. Masood, and A. Yasmin, *Prostate cancer and glutathione S-transferase deletions.* EXCLI Journal, 2015. **14**: p. 1049-1054.

260. Childs, S., et al., *Determination of cellular glutathione:glutathione disulfide ratio in prostate cancer cells by high performance liquid chromatography with electrochemical detection.* Journal of Chromatography A, 2016. **1437**: p. 67-73.

261. Ilonen, I.K., et al., *Oxidative stress in non-small cell lung cancer: role of nicotinamide adenine dinucleotide phosphate oxidase and glutathione.* Acta oncologica (Stockholm, Sweden), 2009. **48**(7): p. 1054-1061.

262. Cui, T., et al., *Utilizing glutathione-triggered nanoparticles to enhance chemotherapy of lung cancer by reprograming the tumor microenvironment.* International Journal of Pharmaceutics, 2018. **552**(1-2): p. 16-26.

263. Momin, M.M., et al., *Extended release delivery of erlotinib glutathione nanosponge for targeting lung cancer.* Artificial Cells, Nanomedicine, and Biotechnology, 2018. **46**(5): p. 1064-1075.

264. Tan, S. and G. Wang, *Lung cancer targeted therapy: Folate and transferrin dual targeted, glutathione responsive nanocarriers for the delivery of cisplatin.* Biomedicine & Pharmacotherapy, 2018. **102**: p. 55-63.

265. Luo, Y.-L., et al., *Differential in situ sensing of extra- and intracellular glutathione by a novel redox-responsive silica matrix-Au nanoprobe.* Analytica Chimica Acta, 2016. **902**: p. 196-204.

266. Grover, A., et al., *Brain-Targeted Delivery of Docetaxel by Glutathione-Coated Nanoparticles for Brain Cancer.* AAPS PharmSciTech, 2014. **15**(6): p. 1562-1568.

267. Lu, Y., et al., *Glutathione-depletion mesoporous organosilica nanoparticles as a self-adjuvant and Co-delivery platform for enhanced cancer immunotherapy.* Biomaterials, 2018. **175**: p. 82-92.

268. Ling, X., et al., *Glutathione-Responsive Prodrug Nanoparticles for Effective Drug Delivery and Cancer Therapy.* ACS nano, 2019. **13**(1): p. 357-370.

269. Phillips, D.J., et al., *Glutathione-triggered disassembly of isothermally responsive polymer nanoparticles obtained by nanoprecipitation of hydrophilic polymers.* Polymer Chemistry, 2014. **5**(1): p. 126-131.

270. Arno, M.C., et al., *Exploiting topology-directed nanoparticle disassembly for triggered drug delivery.* Biomaterials, 2018. **180**: p. 184-192.

271. Li, H., et al., *Reduction-responsive drug delivery based on mesoporous silica nanoparticle core with crosslinked poly(acrylic acid) shell.* Materials Science & Engineering C, 2013. **33**(6): p. 3426-3431.

272. Suk, J.S., et al., *PEGylation as a strategy for improving nanoparticle-based drug and gene delivery.* Advanced drug delivery reviews, 2016. **99**(Pt A): p. 28-51.

273. Phan, H.T., et al., *Investigation of Bovine Serum Albumin (BSA) Attachment onto Self-Assembled Monolayers (SAMs) Using Combinatorial Quartz Crystal Microbalance with Dissipation (QCM-D) and Spectroscopic Ellipsometry (SE).* PLoS One, 2015. **10**(10): p. e0141282.

274. Goncharov, N.V., et al., *Serum Albumin Binding and Esterase Activity: Mechanistic Interactions with Organophosphates.* Molecules, 2017. **22**(7).

275. Kokubo, T., et al., *A hydrolytic enzymelike behavior or bovine serum albumin in hydrolysis of p-nitrophenyl esters.* Tetrahedron Letters, 1982. **23**(15): p. 1593-1596.

276. Tri Giang, P., et al., *Immune complex relay by subcapsular sinus macrophages and noncognate B cells drives antibody affinity maturation.* Nature Immunology, 2009. **10**(7): p. 786.

277. Mishra, S., et al., *Chapter 10 - Carbohydrate-Based Therapeutics: A Frontier in Drug Discovery and Development*, in *Studies in Natural Products Chemistry*, R. Atta ur, Editor. 2016, Elsevier. p. 307-361.

278. Udipi, K., *6 - Stent coatings for blood compatibility*, in *Biosynthetic Polymers for Medical Applications*, L. Poole-Warren, P. Martens, and R. Green, Editors. 2016, Woodhead Publishing. p. 145-169.

279. Sahoo, K., et al., *Nanoparticle Attachment to Erythrocyte Via the Glycophorin A Targeted ERY1 Ligand Enhances Binding without Impacting Cellular Function.* Pharmaceutical Research, 2016. **33**(5): p. 1191-1203.

280. Jachimska, B. and A. Pajor, *Physico-chemical characterization of bovine serum albumin in solution and as deposited on surfaces.* Bioelectrochemistry, 2012. **87**: p. 138-146.

281. Honary, S. and F. Zahir, *Effect of Zeta Potential on the Properties of Nano-Drug Delivery Systems - A Review (Part 2).* Tropical Journal of Pharmaceutical Research, 2013. **12**(2).

282. Cafaggi, S., et al., *Preparation and evaluation of nanoparticles made of chitosan or N- trimethyl chitosan and a cisplatin-alginate complex.* Journal of Controlled Release, 2007. **121**(1-2): p. 110-123.

283. Amiji, M., D. Shenoy, and S. Kommareddy, *Long-Circulating Polymeric Nanoparticles for Drug and Gene Delivery to Tumors*. 2006. p. 231-242.

284. Yang, R., et al., *Lung-Specific Delivery of Paclitaxel by Chitosan-Modified PLGA Nanoparticles Via Transient Formation of Microaggregates.* Journal of Pharmaceutical Sciences, 2009. **98**(3): p. 970-984.

285. Hester, K., et al., *Polyionic complexes of butyrylcholinesterase and poly-l-lysine-g-poly(ethylene glycol): Comparative kinetics of catalysis and inhibition and inB vitro inactivation by proteases and heat.* Chemico-Biological Interactions, 2017. **275**: p. 86-94.

286. Yuan, X., et al., *Characterization of stable lysozyme-entrapped polyion complex (PIC) micelles with crosslinked core by glutaraldehyde.* Polymer, 2005. **46**(18): p. 7749-7758.

287. Hsu, H.-J., et al., *Dendritic PEG outer shells enhance serum stability of polymeric micelles.* Nanomedicine: Nanotechnology, Biology, and Medicine, 2018. **14**(6): p. 1879-1889.

288. Dombkowski, A.A., K.Z. Sultana, and D.B. Craig, *Protein disulfide engineering*. 2014. p. 206-212.

289. Craig, D.B. and A.A. Dombkowski, *Disulfide by Design 2.0: a web-based tool for disulfide engineering in proteins.* BMC Bioinformatics, 2013. **14**(1): p. 346.

290. Creighton, T.E., *Proteins : structures and molecular properties*. 2nd ed.. ed. 1993, New York: New York : W.H. Freeman.

291. Qian, W. and S. Krimm, *Energetics of the disulfide bridge: An ab initio study.* Biopolymers, 1993. **33**(10): p. 1591-1603.

292. Rothwarf, D.M. and H.A. Scheraga, *Equilibrium and kinetic constants for the thiol-disulfide interchange reaction between glutathione and dithiothreitol.* Proceedings of the National Academy of Sciences of the United States of America, 1992. **89**(17): p. 7944.

293. Lee, H., et al., *Reducing agents affect inhibitory activities of compounds: results from multiple drug targets.* Analytical biochemistry, 2012. **423**(1): p. 46-53.

294. Damgaard, D., et al., *Reduced glutathione as a physiological co-activator in the activation of peptidylarginine deiminase.* Arthritis research & therapy, 2016. **18**(1): p. 102-102.

295. Lambert, W., et al., *Thiol-exchange in DTSSP crosslinked peptides is proportional to cysteine content and precisely controlled in crosslink detection by two-step LC-MALDI MSMS.* Protein Science, 2011. **20**(10): p. 1682-1691.

296. Gorman, J.J., T.P. Wallis, and J.J. Pitt, *Protein disulfide bond determination by mass spectrometry.* Mass Spectrometry Reviews, 2002. **21**(3): p. 183-216.

297. Yang, M., C. Dutta, and A. Tiwari, *Disulfide-Bond Scrambling Promotes Amorphous Aggregates in Lysozyme and Bovine Serum Albumin.* The Journal of Physical Chemistry B, 2015. **119**(10): p. 3969-3981.

298. Bennett, K.L., et al., *Chemical cross-linking with thiol-cleavable reagents combined with differential mass spectrometric peptide mapping—A novel approach to assess intermolecular protein contacts.* Protein Science, 2000. **9**(8): p. 1503-1518.

299. Lee, S.Y. and H.-J. Cho, *Dopamine-conjugated poly(lactic-co-glycolic acid) nanoparticles for protein delivery to macrophages.* Journal of Colloid And Interface Science, 2017. **490**: p. 391-400.

300. Gu, Z., et al., *Tailoring nanocarriers for intracellular protein delivery.* Chemical Society reviews, 2011. **40**(7): p. 3638.

301. Kataoka, K. and S. Katayose, *Water-soluble polyion complex associates of DNA and PEG-P(L-lysine) block copolymer.* Polymer Preprints, Division of Polymer Chemistry, American Chemical Society, 1997. **38**(1): p. 547-548.

302. Gustafson, H.H., et al., *Nanoparticle uptake: The phagocyte problem.* Nano Today, 2015. **10**(4): p. 487-510.

303. Maisie J. Joralemon, S.M.a.T.E., *PEGylated polymers for medicine: from conjugation to self-assembled systems.* ChemComm, 2010. **46**: p. 1377–1393.

304. Allen, C., D. Maysinger, and A. Eisenberg, *Nano-engineering block copolymer aggregates for drug delivery.* Colloids and Surfaces B: Biointerfaces, 1999. **16**(1-4): p. 3-27.

305. Otsuka, H., Y. Nagasaki, and K. Kataoka, *Self-assembly of poly(ethylene glycol)-based block copolymers for biomedical applications.* Current Opinion in Colloid & Interface Science, 2001. **6**(1): p. 3-10.

306. Baber, M., *Synthesis of inorganic nanoparticles using microfluidic devices.* 2017, UCL (University College London).

307. Shang-Ming, H., et al., *An Efficient Approach for Lipase-Catalyzed Synthesis of Retinyl Laurate Nutraceutical by Combining Ultrasound Assistance and Artificial Neural Network Optimization.* Molecules, 2017. **22**(11): p. 1972.

308. Dong, Z., et al., *Continuous Ultrasonic Reactors: Design, Mechanism and Application.* Materials, 2020. **13**(2).

309. Fang, Y., et al., *Cleavable PEGylation: a strategy for overcoming the "PEG dilemma" in efficient drug delivery*. 2017. p. 22-32.
310. Carey Pope, C.U., Nicholas Flynn, Kirstin Poindexter, Liyi Geng, and S.H. W. Stephen Brimijoin, Ashish Ranjan, Joshua D. Ramsey, Jing Liu, *In vitro characterization of cationic copolymer-complexed recombinant human butyrylcholinesterase*. Biochemical Pharmacology, 2015. **98**: p. 531-539.

VITA

Joshua Seaberg

Candidate for the Degree of

Master of Science

Thesis: POLY(L-LYSINE)-GRAFTED-POLY(ETHYLENE GLYCOL) NANOPARTICLES FOR DELIVERY OF PROTEINS: EFFECTS OF STIMULUS-RESPONSIVE CROSSLINKING AND TUNABLE MILLIFLUIDIC ASSEMBLY

Major Field: Chemical Engineering

Biographical:

    Education:

    Completed the requirements for the Master of Science in Chemical Engineering at Oklahoma State University, Stillwater, Oklahoma in May 2020.

    Completed the requirements for the Bachelor of Science in Chemical Engineering at Oklahoma State University, Stillwater, Oklahoma in May 2018.

    Experience:

August 2018-Present:	Lead Teaching Assistant for ENSC 3233, Fluid Mechanics Online Section
May-August 2017:	Civil Design Intern in Water and Wastewater at Shive-Hattery, Inc.
May-July 2016:	Civil Design Intern in Water and Wastewater at Shive-Hattery, Inc.
May-July 2015:	Test Engineer Intern at Sears Manufacturing Company

    Professional Memberships:

    American Institute of Chemical Engineers
    Chemical Engineering Graduate Student Association